Deconstructing the integrated oscillator model for pancreatic β -cells

Bertram, Richard; Marinelli, Isabella; Fletcher, Patrick A.; Satin, Leslie S.; Sherman, Arthur S.

DOI:
10.1016/j.mbs.2023.109085

Document Version
Publisher's PDF, also known as Version of record

Citation for published version (Harvard):
Bertram, R, Marinelli, I, Fletcher, PA, Satin, LS & Sherman, AS 2023, 'Deconstructing the integrated oscillator model for pancreatic β -cells', *Mathematical biosciences*, vol. 365, 109085.
https://doi.org/10.1016/j.mbs.2023.109085

Mathematical Biosciences 365 (2023) 109085

Contents lists available at ScienceDirect

Mathematical Biosciences

journal homepage: www.elsevier.com/locate/mbs

Perspective

Deconstructing the integrated oscillator model for pancreatic β-cells

Richard Bertram [a,*], Isabella Marinelli [b], Patrick A. Fletcher [c], Leslie S. Satin [d], Arthur S. Sherman [c]

[a] Department of Mathematics and Programs in Neuroscience and Molecular Biophysics, Florida State University, Tallahassee, FL, United States
[b] Centre for Systems Modeling and Quantitative Biomedicine, University of Birmingham, United Kingdom
[c] Laboratory of Biological Modeling, National Institutes of Health, Bethesda, MD, United States
[d] Department of Pharmacology and Brehm Center for Diabetes Research, University of Michigan Medical School, Ann Arbor, MI, United States

ARTICLE INFO

Keywords:
Beta-cells
Electrical bursting
Fast/slow analysis
Islets

ABSTRACT

Electrical bursting oscillations in the β-cells of pancreatic islets have been a focus of investigation for more than fifty years. This has been aided by mathematical models, which are descendants of the pioneering Chay–Keizer model. This article describes the key biophysical and mathematical elements of this model, and then describes the path forward from there to the Integrated Oscillator Model (IOM). It is both a history and a deconstruction of the IOM that describes the various elements that have been added to the model over time, and the motivation for adding them. Finally, the article is a celebration of the 40th anniversary of the publication of the Chay–Keizer model.

1. Introduction

Teresa Chay and Joel Keizer developed and published the first biophysical model of electrical bursting activity and Ca^{2+} oscillations in pancreatic β-cells in 1983 [1], based on the hypothesis of Atwater and Rojas that slow negative feedback by intracellular Ca^{2+} drives bursting through actions on Ca^{2+}-activated K^+ channels [2]. In the 40 years since, many β-cell modeling papers have appeared, almost all of which were influenced by the *Chay–Keizer model* [3–13]. (See [14] for a recent review of single-cell and whole-islet models.) John Rinzel simplified the model, and used it to perform pioneering work on the analysis of bursting oscillations by decomposing the system of equations into fast and slow subsystems [15]. This *fast–slow analysis*, in which each subsystem is analyzed independently and then stitched together to understand the full bursting dynamics, has been used in most subsequent studies of bursting electrical activity [16–25]. In short, the Chay–Keizer model has been very influential from both biological and mathematical perspectives. The only limitation of the model, which was unavoidable was the incomplete knowledge of β-cell ionic currents at the time the model was developed.

This article mainly tells the story of one mathematical model for bursting in β-cells that was developed over the past two decades, and whose origin can be traced back to the Chay–Keizer model. This *Integrated Oscillator Model (IOM)* continues to evolve, but the 40th anniversary of the Chay–Keizer model that started it all is a good time to look back over the long and winding road that led to the IOM in its current form. The model includes components for electrical activity and intracellular Ca^{2+} handling, as well as metabolism, which is coupled to both. It is able to account for *fast bursting* with a period of tens of seconds as well as *slow bursting* with a period of several minutes. Both forms of bursting are commonly observed in mouse islets [26–29], as is a hybrid of the two called *compound bursting* that consists of slow episodes of fast bursts [28,30–32].

The model name comes from the co-existence of two oscillation mechanisms, one based on mutual interactions between intracellular Ca^{2+} and the cell's electrical subsystem, and the other based on an intrinsic glycolytic oscillator. In the initial version of the model the two oscillators were weakly coupled, motivating the original name *Dual Oscillator Model* [33]. More recent experimental data led to revisions that increased the coupling strength between the two oscillators so that they are more integrated, motivating the current model name [34]. In this article, we describe the evolution of the model, as well as the mathematical underpinnings of the model dynamics.

2. The Chay–Keizer model

In its original form [1], the Chay–Keizer model is 5-dimensional, with differential equations for the membrane potential (V), two activation and one inactivation variables, and the free intracellular Ca^{2+} concentration (c). The essential dynamics can, however, be produced with a three-dimensional version that includes differential equations for V, the fraction of open K^+ channels (n), and c. This reduced model

* Corresponding author.
E-mail address: bertram@math.fsu.edu (R. Bertram).

https://doi.org/10.1016/j.mbs.2023.109085
Received 21 July 2023; Received in revised form 12 September 2023; Accepted 26 September 2023
Available online 4 October 2023

simplifies the analysis, is used in the IOM, and replicates the results of the original model. The differential equations are:

$$\frac{dV}{dt} = -[I_{Ca} + I_K + I_{K(Ca)} + I_{K(ATP)}]/C_m \quad (1)$$

$$\frac{dn}{dt} = \frac{n_\infty(V) - n}{\tau_n} \quad (2)$$

$$\frac{dc}{dt} = f_c J_{mem} \ . \quad (3)$$

The right hand side of the V equation (Eq. (1)) is the sum of the ionic currents, divided by the membrane capacitance (a parameter). The first term (I_{Ca}) is an inward Ca^{2+} current that depolarizes the membrane and produces the upstroke of an action potential. It activates rapidly, and its activation state is assumed to change instantaneously with V. The second term (I_K) is the outward delayed rectifying current, which is responsible for the downstroke of an action potential. Its activation occurs on a slower time scale, and is therefore described by a differential equation.

Equations for these spiking currents, which resemble those of Hodgkin and Huxley for conductances of the squid giant axon [35] are:

$$I_{Ca} = g_{Ca} m_\infty(V)(V - V_{Ca}) \quad (4)$$

$$I_K = g_K n (V - V_K) \quad (5)$$

where g_{Ca} and g_K are maximum conductance parameters, $m_\infty(V)$ is the equilibrium fraction of open Ca^{2+} channels, and n is the fraction of open delayed rectifying K^+ channels with dynamics described by Eq. (2). The V-dependent equilibrium activation functions are increasing sigmoids:

$$m_\infty(V) = \frac{1}{1 + \exp\left(\frac{v_m - V}{s_m}\right)} \quad (6)$$

$$n_\infty(V) = \frac{1}{1 + \exp\left(\frac{v_n - V}{s_n}\right)} \quad (7)$$

where v_m and v_n are parameters that set the half-maximum, and s_m and s_n set the slope of the sigmoids.

The third term ($I_{K(Ca)}$) in the V equation describes the ionic current through Ca^{2+}-activated K^+ channels, in which the channel gating is determined by the intracellular Ca^{2+} concentration rather than the membrane potential. The time dynamics of the conductance is therefore dictated by the dynamics of the intracellular Ca^{2+} concentration, and channel activation is described by a Hill function that increases with c. This current is:

$$I_{K(Ca)} = g_{K(Ca)} \left(\frac{c^{n_k}}{K_d^{n_k} + c^{n_k}}\right)(V - V_K) \quad (8)$$

where $g_{K(Ca)}$ is a parameter for the maximal conductance, nk is the Hill coefficient, and the parameter K_d sets the half-activation point. As we shall see shortly, this current plays a key role in the production of bursting.

The fourth term ($I_{K(ATP)}$) in the V equation was not in the original Chay–Keizer model, since it describes an ionic current that had not yet been discovered when the Chay–Keizer model was published in 1983. This current, through ATP-sensitive K^+ channels, was shown in 1984 to be directly inhibited by glucose metabolism [36,37]. It was later shown to be activated by adenosine diphosphate (ADP) and inhibited by adenosine triphosphate (ATP), so that its activation state depends approximately on the ratio of the nucleotide concentration, i.e., ATP/ADP [38]. As we shall see later, temporal variation of ATP/ADP and its effect on current through K(ATP) channels plays a major role in the production of slow bursting, but since the focus of the Chay–Keizer model was on fast bursting, we include the current here only as an additional K^+ current with constant conductance. The K(ATP) current used in this model is then:

$$I_{K(ATP)} = g_{K(ATP)}(V - V_K) \quad (9)$$

where $g_{K(ATP)}$ is a conductance parameter.

Table 1
Chay–Keizer model parameter values.

Parameter	Value	Parameter	Value
g_{Ca}	1000 pS	g_K	2700 pS
$g_{K(Ca)}$	400 pS	$g_{K(ATP)}$	180 pS
C_m	5300 fF	τ_n	20 ms
f_c	0.001	α	1.125×10^{-6} μmol fA^{-1} $l^{-1}ms^{-1}$
k_{pmca}	0.045 ms^{-1}	K_d	0.3 μM
V_{Ca}	25 mV	V_K	−75 mV
v_m	−20 mV	v_n	−16 mV
s_m	12 mV	s_n	5 mV
n_k	3		

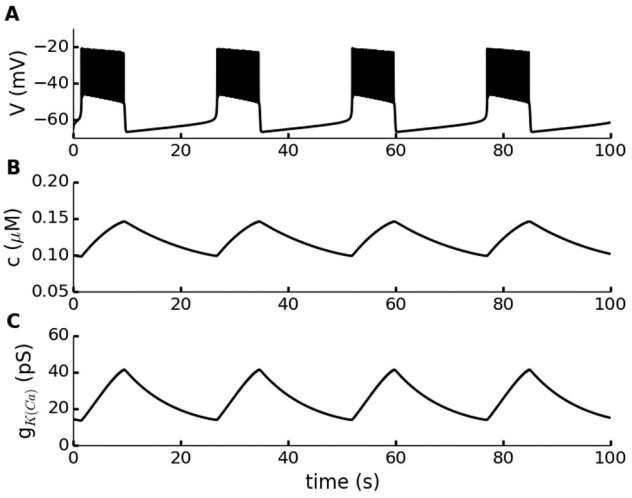

Fig. 1. Bursting produced by a 3-dimensional Chay–Keizer model. **(A)** Fast bursting, consisting of active phases where the model cell is spiking and silent phases where it is hyperpolarized. **(B)** The free intracellular Ca^{2+} concentration has a slow sawtooth pattern, rising during each burst active phase and declining during each silent phase. **(C)** The K(Ca) conductance responds to the Ca^{2+} concentration, exhibiting a similar sawtooth pattern. Parameter values are given in Table 1.

The right hand side of the c differential equation (Eq. (3)) has a single term for the net flux of Ca^{2+} across the plasma membrane (J_{mem}) multiplied by the fraction of Ca^{2+} that is in a free state (f_c). The influx of Ca^{2+} into the cell is through Ca^{2+} channels, so is proportional to I_{Ca}. The efflux is through plasma membrane Ca^{2+} pumps, and this efflux is assumed to be proportional to c. Thus, the net Ca^{2+} flux is:

$$J_{mem} = -(\alpha I_{Ca} + k_{pmca} c) \quad (10)$$

where α is a parameter that converts current to flux, and k_{pmca} is a parameter for the pumping strength.

Calcium dynamics drive fast bursting

The Chay–Keizer model produces fast electrical bursting (Fig. 1A) due to the slow buildup of free intracellular Ca^{2+} (Fig. 1B) that periodically terminates electrical spiking through the activation of K(Ca) channels (Fig. 1C). The Ca^{2+} concentration builds up because of influx through voltage-dependent Ca^{2+} channels. Once the outward current through K(Ca) channels reaches a sufficiently high level, the membrane potential no longer reaches the spike threshold and the burst of action potentials ends. The cell then enters a silent phase, during which Ca^{2+} removal through plasma membrane pumps slowly reduces c and the K(Ca) conductance. Once this conductance becomes sufficiently small, the membrane potential again reaches the spike threshold, terminating the burst silent phase and starting a new burst active phase.

There are two important things to note about the bursting in Fig. 1. The first is that c changes on a much slower time scale than V (and the activation variable n, which is not shown). The second is that for the

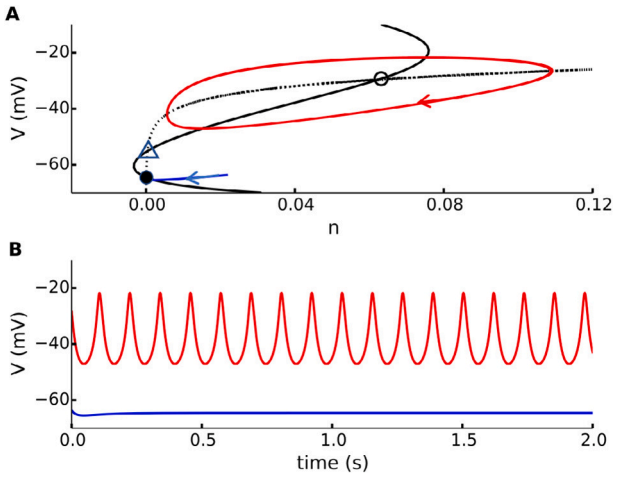

Fig. 2. Bistable dynamics of the Chay–Keizer fast subsystem, with $c = 0.12$ μM. **(A)** Phase portrait showing the V nullcline (black, solid), n nullcline (black, dotted), a continuous spiking limit cycle (red), and a trajectory leading to the stable node (blue). The equilibrium points are a stable node (black, filled circle), an unstable spiral (black, unfilled circle), and a saddle point (black, unfilled triangle). **(B)** Time courses of the continuous spiking limit cycle (red) and trajectory (blue) leading to the low-V stable equilibrium. Parameter values are given in Table 1.

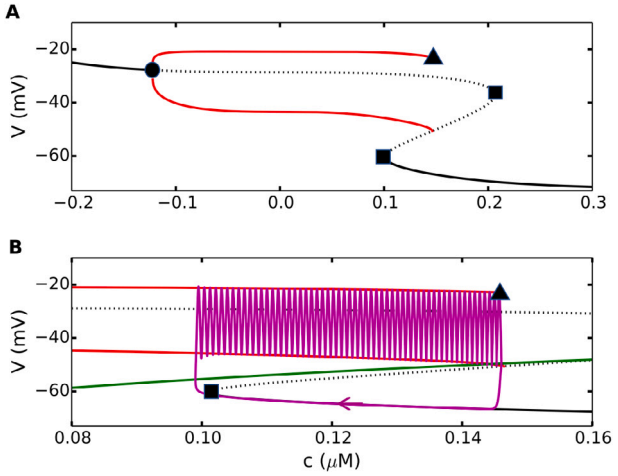

Fig. 3. Fast–slow analysis of the 3-dimensional Chay–Keizer model. **(A)** Bifurcation diagram of the fast subsystem. Stable (solid) and unstable (dotted) equilibria are in black. The minimum and maximum V of the stable periodic spiking solutions are in red. There is a subcritical Hopf bifurcation (filled circle), two saddle–node bifurcations (squares), and a homoclinic bifurcation (triangle). **(B)** The c-nullcline (green) is superimposed on the bifurcation diagram. Also superimposed is the burst trajectory (magenta). Parameter values are given in Table 1.

same value of c the model cell can either be spiking or silent. That is, if the *slow variable* c were to be held fixed at any value taken on during bursting, the *fast subsystem* (V and n) would be bistable.

The fast-subsystem dynamics can be viewed in the (n, V) phase plane, as in Fig. 2A. This shows three intersections of the n nullcline (black, dotted line) and cubic-like V nullcline (black, solid line), corresponding to a stable node (the silent state), an unstable spiral at a depolarized voltage, and a saddle point. In addition to the stable equilibrium, there is a stable limit cycle (in red) surrounding the unstable spiral, corresponding to a periodic spiking state. The basins of attraction of these two attractors are separated by the stable manifold of the saddle point. Time courses leading to the two attractors are shown in Fig. 2B.

This description of the fast subsystem dynamics is for an appropriately-chosen value of the slow variable c. A summary of the asymptotic dynamics of the fast subsystem over a large range of values of c is shown with a bifurcation diagram, treating c as the bifurcation parameter, in Fig. 3A. (The diagram extends into negative non-physical values of c.) There are two intervals in which the equilibrium is stable, indicated by the solid black branches of the diagram. There is also a branch of stable periodic spiking solutions, indicated in the diagram with two red curves (the minimum and maximum voltage values taken on during the oscillation). Branches are born or change stability at a subcritical Hopf bifurcation (circle), two saddle–node bifurcations (squares), and a homoclinic bifurcation in which the period of the spiking solution approaches infinity (triangle). A key feature of the diagram is an interval of bistability between the left saddle–node and the homoclinic bifurcation. The value of c used in Fig. 2 falls within this interval, which is necessary, but not sufficient, for bursting in the Chay–Keizer model.

To perform a fast–slow analysis, one treats the fast-subsystem bifurcation diagram, often referred to as the *critical manifold*, as a generalized V-nullcline. In this spirit, the c-nullcline is superimposed onto the diagram (Fig. 3B, focusing now on the bistable interval). As with a standard phase plane analysis, one can use the curves to determine the flow of the trajectory in the (c, V) plane, noting that horizontal flow is much slower than vertical flow since c changes slowly compared to V. The burst trajectory, superimposed in magenta, can then be understood in terms of this flow much in the same way that relaxation oscillations are analyzed in the phase plane. During the silent phase of the burst, the trajectory follows the lower stable branch of the manifold (acting as the nullcline of the fast variable V) until it terminates at a saddle–node bifurcation. From here, the trajectory moves upward to the stable periodic spiking branch. Since it has crossed the c-nullcline, the direction of flow switches from left to right, so the trajectory moves rightward along the spiking branch until it terminates at a homoclinic bifurcation. This is the active phase of the burst. Once the trajectory passes through the homoclinic bifurcation, it moves downward to the stable stationary branch and the flow switches to the left as it begins a new silent phase. The burst is a complex stable limit cycle, but as we see here, it can be clearly understood with the aid of the critical manifold and the slow-variable nullcline. This fast–slow analysis of bursting, pioneered by John Rinzel [22], has been applied to many models of bursting [25,39].

The Chay–Keizer model provides an explanation for the glucose response

The function of pancreatic β-cells is to transduce the blood glucose level into insulin secretion, so that more insulin is secreted when the glucose level is elevated. A primary way of doing this is to regulate the cell's electrical activity. When the glucose is at a subthreshold level, the cell is electrically silent. When it is at a stimulatory level and the cell is bursting, an increase in the glucose level increases the duration of the burst active phase relative to the silent phase. When the glucose level is very high, the cell spikes continuously. This glucose modulation of activity can be described in terms of the burst *plateau fraction*, which is the ratio of the active phase duration to the entire burst period. Islet studies have shown that the plateau fraction rises monotonically from 0 to 1 as the glucose level is increased [40]. In addition to demonstrating a plausible mechanism for bursting electrical activity, the Chay–Keizer model also provided a plausible mechanism for this fundamental feature of β-cell electrical activity. Glucose is transported into the cell and metabolized to ATP. At the time that the model was published, it was not known that there are K^+ channels that are closed by ATP, so Chay and Keizer proposed that the ATP increases the activity of plasma membrane Ca^{2+} pumps via hydrolysis. In terms of the model, this means that an increase in the glucose level would increase the parameter k_{pmca}. The effect of doing this is shown in Fig. 4A. For a bursting model cell, increasing glucose increases the active phase duration while decreasing the silent phase duration, as

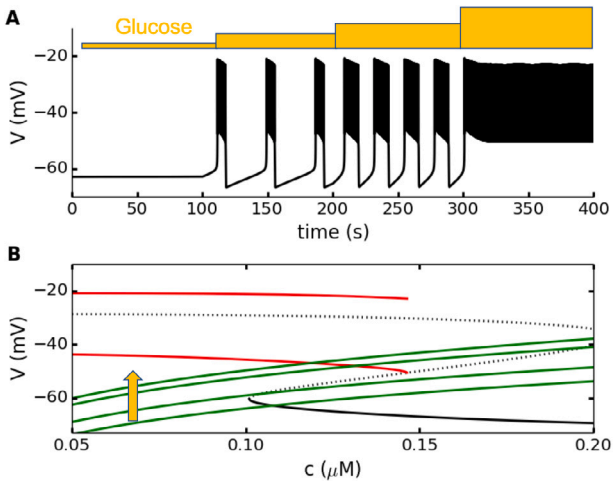

Fig. 4. Explanation for the response to glucose in the Chay–Keizer model. **(A)** Increases in the extracellular glucose concentration are simulated by increasing the parameter for the activity of plasma membrane Ca^{2+} pumps, k_{pmca}. In this simulation, k_{pmca} (units of ms^{-1}) is increased from 0.025, to 0.035, to 0.055, and finally to 0.065 as indicated. **(B)** The fast-subsystem bifurcation diagram is unaffected by the change in k_{pmca}, which only acts by shifting the c-nullcline upward. Parameter values are given in Table 1.

Fig. 5. Recording of the intracellular Ca^{2+} concentration from a mouse pancreatic islet using the fluorescent dye fura-2. The Ca^{2+} profile has a sharp rise at the beginning of a burst, followed by a plateau, and then an initial sharp decline followed by a slow falloff during the silent phase. This is in contrast with the sawtooth shape predicted by the Chay–Keizer model (Fig. 1).
Source: Reproduced from [28].

in experiments. At the highest level shown the bursting is replaced by continuous spiking.

This effect can be understood nicely using fast–slow analysis. Since the k_{pmca} parameter does not appear in either the V or the n differential equation, changing it has no impact on the fast-subsystem bifurcation diagram. It only appears in the c differential equation, and impacts c in part by shifting the c-nullcline upward when k_{pmca} is increased (Fig. 4B). At the lowest value, $k_{pmca} = 0.025$ ms^{-1}, the nullcline intersects the bottom branch of the critical manifold. This intersection is an equilibrium of the full system of equations, and since the bottom branch is stable so too is this equilibrium. As a result, the model cell is silent. When k_{pmca} is increased to 0.035 ms^{-1}, the intersection with the critical manifold is on the unstable middle branch, so the full-system equilibrium is unstable. In this case, a bursting oscillation is produced as shown in Fig. 3B. Bursting also occurs with the higher value $k_{pmca} = 0.055$ ms^{-1}. The c-nullcline is shifted upward even higher, but the burst trajectory, when superimposed on the critical manifold, looks very similar to Fig. 3B. The burst active phase starts at the lower knee (saddle–node bifurcation) and ends near where the periodic branch meets the unstable middle branch of the critical manifold (homoclinic bifurcation), just as before. All that changes when the c-nullcline is raised is the speed at which the trajectory moves through the two phases of the burst. When the phase point travels along the lower branch of the critical manifold during the silent phase it is further from the equilibrium c value and moves faster with the larger value of k_{pmca}. When traveling along the periodic branch during the active phase, the phase point is now closer to the c-nullcline, so it moves more slowly. As a result, the silent phase is now shorter and the active phase longer with the larger k_{pmca} value and the plateau fraction is thus greater. Finally, at the highest value of k_{pmca} shown the c-nullcline intersects deep into the periodic branch, trapping the trajectory in the spiking state. It no longer cycles between the bottom branch and periodic branch of the critical manifold, but instead stays on the periodic branch. (The third c-nullcline also intersects the periodic branch, and if the time scale separation were increased the phase point would also get stuck here in the continuous spiking state [41].)

3. Phantom bursting models

Sawteeth and square waves

Despite the impact that the Chay–Keizer model has had on the understanding of bursting in β-cells and fast–slow analysis, it became apparent shortly after its publication that the model was wrong, or at least fundamentally incomplete. Once fluorescent dyes for Ca^{2+} were developed and used with islets, it was clear that the Ca^{2+} traces did not have the sawtooth shape predicted by the Chay–Keizer model (Fig. 1B), but instead had more of a square-wave shape, with a slow decline at the end of each burst (Fig. 5). Indeed, the Ca^{2+} concentration looked more like a fast variable than a slow one. Making Ca^{2+} into a fast variable is easily achieved, by increasing the fraction of Ca^{2+} that is free from 0.001 to the more realistic value of 0.01 (as in Table 2), but then the model cell does not burst, and even with parameter changes any bursting that is achieved has a much smaller period. The observation that c is not a slow variable prompted the development of a number of other models postulating different slow variables, such as the inactivation of Ca^{2+} channels [10], the ATP/ADP ratio acting through K(ATP) channels [9,42], and the activity-dependent variation in Na^+ and K^+ concentrations and their impact on electrogenic ion pumps [7,43,44]. However, Teresa Chay found a way to rescue the Chay–Keizer model while retaining the K(Ca) current as the key electrical current underlying bursting [6]. This was done by adding a second Ca^{2+} compartment, the endoplasmic reticulum (ER), which acts as an intracellular Ca^{2+} store. During the burst active phase the Ca^{2+} concentration in the ER (c_{ER}) slowly builds up, and during the silent phase, the ER slowly releases Ca^{2+} into the cytosol. This allows the cytosolic Ca^{2+} concentration to be fast, but with slow components due to modulation by the ER Ca^{2+} concentration, which becomes the slow variable dictating the start and end of each burst active phase. Experiments reported 15 years later confirmed that slow oscillations in c_{ER} indeed occur during bursting [45].

The faster dynamics and square-wave shape of c solve another problem: although the original Chay–Keizer model successfully explained the increased plateau fraction when glucose concentration is increased, this does not lead to higher Ca^{2+} concentration when the time course is a sawtooth. With a square-wave shape, the average Ca^{2+} concentration does increase and can account for increased insulin secretion.

A version of the Chay–Keizer model with an ER-Ca^{2+} compartment was later implemented in a model from our group [4]. The V and n differential equations are the same as Eq. (1), (2), but now there are two Ca^{2+} concentration equations, for the cytosol and the ER:

$$\frac{dc}{dt} = f_c(J_{mem} + J_{ER}) \tag{11}$$

$$\frac{dc_{ER}}{dt} = -f_c\sigma_v J_{ER}\,. \tag{12}$$

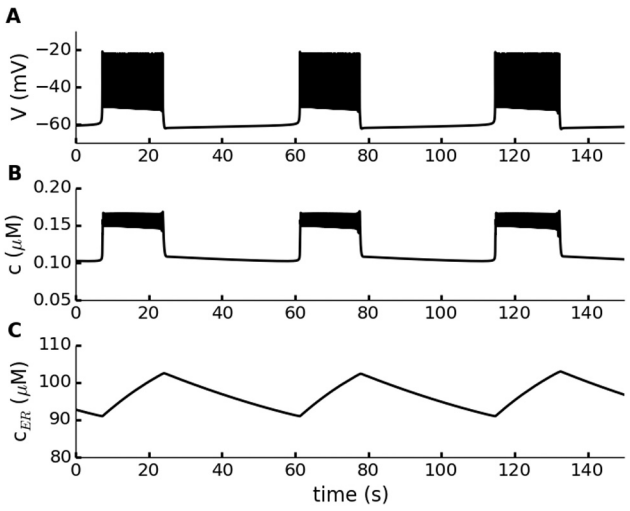

Fig. 6. Bursting produced by a Chay–Keizer model with an added compartment for the Ca^{2+} concentration in the ER. **(A)** Bursting electrical activity. **(B)** The cytosolic Ca^{2+} concentration no longer has a sawtooth pattern, but instead looks more like a square wave. **(C)** The ER Ca^{2+} concentration exhibits a sawtooth pattern; it is the slowest variable in the system. Parameter values are given in Table 2.

Table 2
Parameter values for the Chay–Keizer model with an ER.

Parameter	Value	Parameter	Value
g_{Ca}	1200 pS	g_K	3000 pS
$g_{K(Ca)}$	800 pS	$g_{K(ATP)}$	230 pS
C_m	5300 fF	τ_n	16 ms
f_c	0.01	α	4.5×10^{-6} μmol fA^{-1} l^{-1} ms^{-1}
k_{pmca}	0.2 ms^{-1}	K_d	0.3 μM
V_{Ca}	25 mV	V_K	−75 mV
v_m	−20 mV	v_n	−16 mV
s_m	12 mV	s_n	5 mV
k_{SERCA}	0.4 ms^{-1}	σ_v	5
n_k	5	p_{leak}	0.0005 ms^{-1}

where J_{mem} is the same as before, and the net flux of Ca^{2+} into the cytosol from the ER is

$$J_{ER} = J_{leak} - J_{SERCA} \tag{13}$$

where $J_{leak} = p_{leak}(c_{ER} - c)$ is the leak across the ER membrane and $J_{SERCA} = k_{SERCA}c$ is the flux into the ER through sarcoplasmic endoplasmic reticulum Ca^{2+} (SERCA) pumps. The c_{ER} differential equation includes a parameter for the ratio of volumes of the cytosol and the ER (σ_v). All parameter values are given in Table 2.

This augmented Chay–Keizer model was used to generate Fig. 6, which shows bursts of electrical activity and corresponding Ca^{2+} traces. The cytosolic Ca^{2+} time course looks very different from Fig. 1, with the sawtooth pattern replaced by a square wave. At the end of an active phase, c declines rather than rises, reflecting the exchange of Ca^{2+} from the ER to the cytosol and out of the cell through Ca^{2+} pumps. The Ca^{2+} concentration in the ER is now the variable with a sawtooth time course, since it is the slowest variable of the system.

Understanding phantom bursting using fast–slow analysis

The Chay–Keizer model with ER represents a departure from previous models in the family because it has two slow variables, c and c_{ER}, instead of one. Both contribute to bursting to different degrees, depending on parameters, so the "slow variable" can be viewed as a composite of the two rather than a single physical variable. This gave rise to the term *phantom bursting* [46].

One could perform a fast–slow analysis with either c_{ER} or c as the single slow variable. Since c_{ER} acts on the membrane only through the effect of c on K(Ca) channel conductance, we choose to use a measure of this conductance in the fast–slow analysis. That is, we use

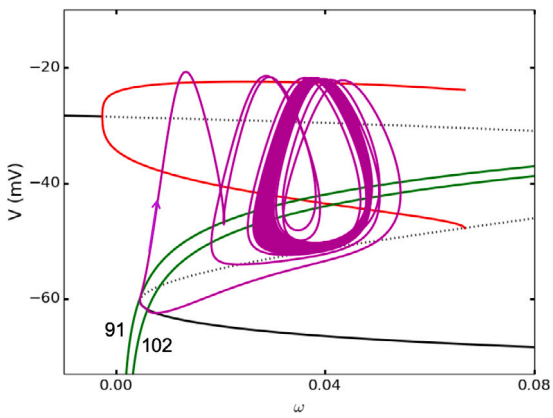

Fig. 7. Fast–slow decomposition of bursting produced by the Chay–Keizer model with an ER compartment. Two ω-nullclines (green) are shown, for c_{ER} = 91 μM and c_{ER} = 102 μM. The latter intersects the bottom branch of the critical manifold, while the former does not. The burst trajectory is superimposed (magenta). Parameter values are given in Table 2.

$$\omega = \frac{c^5}{c^5 + K_d^5} \tag{14}$$

which is the fraction of activated K(Ca) channels in this model. The fast subsystem (V and n) bifurcation diagram is shown in Fig. 7, with the stationary branch in black and the periodic spiking branch in red. During bursting oscillations, c_{ER} varies from 91 to 102 μM, so we compute c nullclines with these two extreme values of c_{ER} (c_{ER} enters the c differential equation through the flux term J_{ER}). These are then transformed to the ω coordinate through Eq. (14) and superimposed on the critical manifold.

At the start of a burst active phase c_{ER} is low, 91 μM, and the nullcline intersects the periodic branch, but not the stable stationary branch. Since with parameter changes c is now a much faster variable than in the Chay–Keizer model, the trajectory does not follow the critical manifold as closely, and at the start of the active phase it moves quickly to the right until it stalls in a spiking state. Now the slow component becomes important, as c_{ER} slowly increases and moves the nullcline rightward. This moves the trajectory in the same direction, building up K(Ca) conductance until the voltage no longer reaches the spike threshold and the trajectory leaves the periodic spiking branch. From here, it travels quickly to the left and stalls at the intersection of the nullcline (now with c_{ER}=102 μM) with the stable stationary branch of the critical manifold. From here it drifts slowly leftward as c_{ER} slowly declines and moves the nullcline leftward. The silent phase terminates when the nullcline moves past the saddle–node bifurcation and the trajectory once again returns to the periodic branch.

In addition to providing a more accurate shape for the time course of c, the phantom bursting mechanism allows for a greater range of burst periods, and in particular, burst periods of several minutes, like the one shown in Fig. 5.

The wide range of burst periods is possible because the period is determined both by the time required for the trajectory to move along a branch of the critical manifold before it stalls, and the time required for the nullcline to move so that the trajectory escapes. In the Chay–Keizer model with an ER, the former reflects the time constant for c, while the latter reflects the much larger time constant for c_{ER}. The deeper the intersection of the nullcline with the periodic or stable stationary branch of the critical manifold, the longer the burst period. Thus, the burst period can be extended to several minutes. In contrast, if the nullcline intersects only the middle, unstable, stationary branch, then

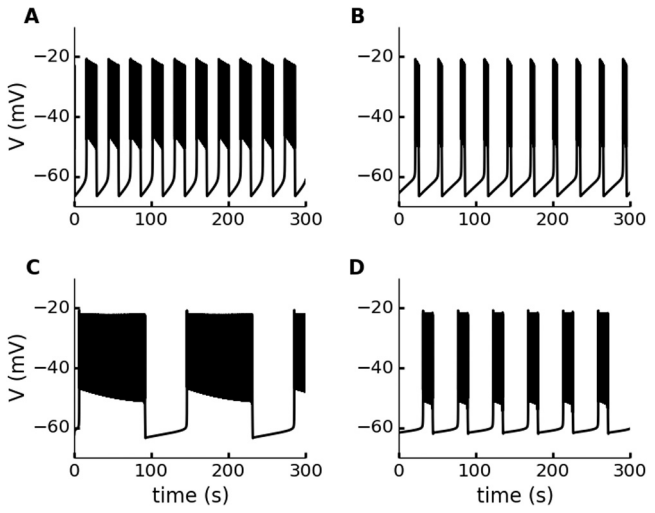

Fig. 8. Burst period varies over a much wider range with a phantom burster than with a standard burst mechanism. **(A, B)** There is a substantial change in the plateau fraction, but not period, when the K(Ca) channel conductance is increased from $g_{K(Ca)} = 250$ pS (left) to 900 pS (right) in the Chay–Keizer model. **(C, D)** There is a substantial change in both plateau fraction and period with the same conductance change in the Chay–Keizer model with an ER. Parameter values for the top and bottom panels are given in Tables 1 and 2, respectively.

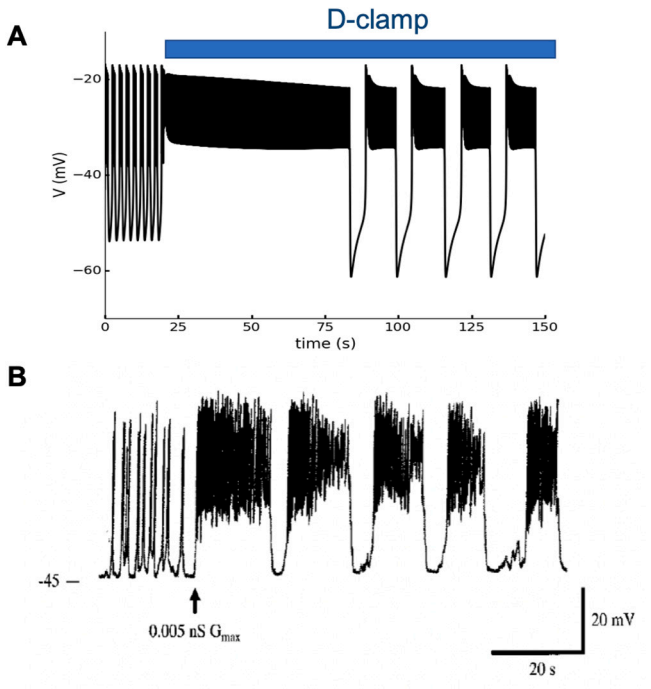

Fig. 9. Adding an appropriate current to a fast bursting cell converts it to a medium burster. **(A)** Model prediction. The model cell is initially bursting at a high frequency, but when the dynamic-clamp current is added ("D-clamp") it switches to medium bursting after a transient. Simulation performed using the original phantom bursting model [46]. The dynamic clamp parameter values are $g_{cmp} = 12$ pS, $V_{cmp} = 100$ mV, $\tau_z = 50$ ms. **(B)** Experimental recording of electrical activity from a β-cell in which a dynamic clamp current with conductance of 5 pS is added at the arrow.
Source: This panel reproduced from [46].

the burst will be driven entirely by changes in c (as in Fig. 3) and the period will be small, just a few seconds.

The enhanced dynamic range of phantom bursting is illustrated in Fig. 8, where the top panels show bursting produced by the Chay–Keizer model with a single slow variable, c, and low and high values of the K(Ca) conductance (panels A and B, respectively). The increase in $g_{K(Ca)}$ has a big impact on the plateau fraction, but little impact on the burst period. In contrast, using the same values for $g_{K(Ca)}$ in the Chay–Keizer model with an ER, a phantom burster, there is a big change in the burst period (panels C and D) because at low values of $g_{K(Ca)}$ the nullcline intersects deep into the periodic and stationary branches, while with high values of $g_{K(Ca)}$ the intersection is shallow.

By using the same values of $g_{K(Ca)}$ for both models we somewhat understate the flexibility provided by phantom bursting. With the Chay–Keizer model, if $g_{K(Ca)}$ is reduced much below 250 pS, the system produces continuous spiking since the nullcline intersects deep into the periodic branch and there is no second slow variable to move it. With the phantom burster, $g_{K(Ca)}$ can continue to be decreased; deeper intersections just means bursting with longer periods, although at some point bursting will transition into continuous spiking. Thus, the burst dynamics are much more flexible with the phantom burster than with a burster relying on a single slow variable such as Chay–Keizer.

Converting from fast to medium bursting using the dynamic clamp technique

Electrical recordings and Ca^{2+} measurements in single β-cells, isolated from islets, typically exhibit very fast oscillations with a period of a couple of seconds [28,47], and much less often slow oscillations with a period of several minutes [48,49]. In contrast, bursting in β-cells within intact islets typically show either "medium" bursting with a period of tens of seconds or slow bursting with a period of several minutes [29]. Why don't single β-cells ever exhibit medium bursting? One hypothesis is that they are not capable of it, either because of channel noise [50,51] or heterogeneity of individual cells [52] and require electrical coupling with other β-cells to do it. Using phantom bursting models, we predicted that single β-cells could in fact produce medium bursting with the addition of an appropriate ionic current.

To test this model prediction, we used the dynamic clamp technique [47,53]. This allows one to add an artificial current to a single cell using the cell's own membrane potential to calculate the current with voltage-dependent conductance. In our test of the model prediction, we added a current

$$I_{cmp} = g_{cmp} z (V - V_{cmp}) \tag{15}$$

where z is an activation variable that satisfies the differential equation

$$\frac{dz}{dt} = \frac{z_\infty(V) - z}{\tau_z} \tag{16}$$

and

$$z_\infty(V) = \frac{1}{1 + \exp\left(\frac{-(22+V)}{7.5}\right)} \tag{17}$$

which is an increasing Hill function of V.

A simulation showing the effect of adding this dynamic-clamp current is in Fig. 9A. This uses the original phantom bursting model [46], in which there are two slow variables, s_1 and s_2. Both are activation variables of K^+ channels, and the activation time constant for the latter is much larger (by a factor of 120) than that of the former. Initially, the model cell is bursting at a very high rate, with a period of 2 s. When the dynamic-clamp current is added the system settles into a burst pattern with period of 16 s. Thus, the current transformed the fast burster to a medium burster. This increase in period did not arise from slow dynamics of the dynamic-clamp current, which had a time constant of only 50 ms. Rather, the added current unmasked an intrinsic slow mechanism by stretching the critical manifold, so that the slow variable nullcline now intersected it on the lower stationary branch and the upper periodic branch, as in Fig. 7. Changes in the second, much slower, variable were therefore required to produce a burst pattern. That is, the bursting that was originally driven by the slow variable s_1, was transformed into phantom bursting in which changes

in the slower variable s_2 were necessary to escape the silent and active phases. The result is medium bursting. Experimental tests of this model prediction reliably showed a similar transition, as illustrated in Fig. 9B. A similar prediction was made using a later phantom bursting model (described above) [28]. In both publications, experimental tests adding the dynamic clamp current suggested by the model reliably resulted in a transition from fast to medium bursting. These are the only examples that we know of in which the medium burst pattern often seen in islets was observed in single β-cells.

4. The dual oscillator model

The great flexibility in burst period provided by phantom bursting seemed to explain the perplexing observation that bursting in β-cells can be very fast in single cells or islets in the presence of acetylcholine (just a few seconds), or somewhat slower in islets (tens of seconds), or very slow in islets and some single cells (several minutes) [26,28,40,47,48,54]. A burst mechanism involving a single slow variable is just not flexible enough to account for this. A phantom burster is.

Despite the success of phantom bursting in explaining bursting in β-cells, there were data that appeared to defy explanation by the model. These electrophysiology data, from three different labs, showed episodes of bursts and cases in which the plateau fraction varied over time in a rhythmic manner [55–57]. We coined the terms *compound bursting* and *accordion bursting* for these two unusual types of electrical behavior. Later electrophysiology and Ca^{2+} imaging data demonstrated that these strange forms of bursting are not so unusual, and compound bursting is commonly seen in islet recordings [32,58,59]. Just as with the slow form of bursting, the episode period, and the period of the rhythmic modulation of plateau fraction, is similar to the 5–10 min period of insulin oscillations in the blood [60]; oscillations with that period enhance the efficacy of insulin action [61]. These compelling data suggested that there could be two co-existing oscillators; one oscillator would produce bursts, and the other would group them together into episodes or slowly vary the plateau fraction of each burst. The *Dual Oscillator Model (DOM)* [32], published in 2004, was a mathematical realization of that idea. In the DOM, there is an *electrical oscillator* based largely on the phantom bursting model of [4], and a separate *glycolytic oscillator* based on [62] that produced a slow oscillation in the ATP/ADP ratio. The oscillations in ATP/ADP affect the cell's electrical activity through K(ATP) channels; an increase in ATP/ADP results in a decrease in $g_{K(ATP)}$, so oscillations in ATP/ADP result in oscillations in $g_{K(ATP)}$.

Glycolytic oscillations

The enzyme underlying glycolytic oscillations in the DOM is phosphofructokinase (PFK). It was demonstrated by Tornheim and collaborators that this enzyme can produce metabolic oscillations in muscle extracts [63] and Tornheim proposed that the same enzyme, which is also found in β-cells, could be responsible for slow oscillations in β-cells [64]. The enzyme acts at an early stage of glycolysis to convert the substrate fructose 6-phosphate (F6P) into fructose 1,6-bisphosphate (FBP). It is an allosteric enzyme that is inhibited by ATP and stimulated by its product FBP. The inhibition of PFK by ATP is the classic negative feedback that limits ATP production. The stimulation by FBP provides positive feedback to PFK, and is not as ubiquitous in biology. One important effect of the positive feedback is that it facilitates oscillations in PFK activity through the substrate depletion mechanism. That is, the PFK activity becomes so high that it largely depletes the substrate. This results in a decline in PFK activity until the substrate level builds back up, at which point another round of FBP production begins with the subsequent buildup of PFK activity, restarting the cycle. Since the dominant PFK enzyme in β-cells is the same isoform as that in muscle, we used the same differential equations for PFK substrate (F6P) and

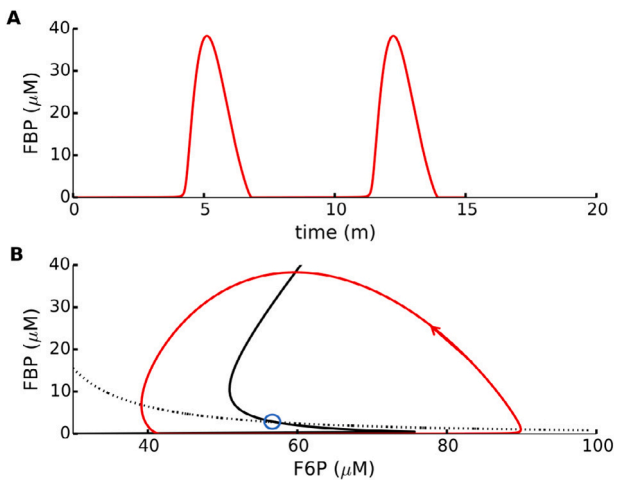

Fig. 10. Oscillations in the concentration of the glycolytic metabolite FBP, produced by the glycolytic enzyme PFK. **(A)** The FBP time course exhibits pulses, with period of 7 min. **(B)** The F6P-nullcline (black dotted curve) and FBP-nullcline (black solid curve) shown in the phase plane. They intersect once at an unstable node (blue circle). The glycolytic oscillation is a limit cycle (red).

product (FBP) that were used in the model for glycolytic oscillations in muscle developed by Smolen [62]:

$$\frac{d\mathrm{F6P}}{dt} = 0.3(J_{\mathrm{GK}} - J_{\mathrm{PFK}}) \tag{18}$$

$$\frac{d\mathrm{FBP}}{dt} = J_{\mathrm{PFK}} - \frac{1}{2}J_{\mathrm{PDH}} \tag{19}$$

where J_{GK} is flux through glucokinase, J_{PFK} is flux through PFK, and J_{PDH} is flux through pyruvate dehydrogenase (PDH), assumed to be proportional to the square root of the FBP concentration:

$$J_{\mathrm{PDH}} = v_{\mathrm{PDH}}\sqrt{\mathrm{FBP}/(1\mu\mathrm{M})}\,. \tag{20}$$

The glycolytic model is from [62], and equations for the flux terms and parameter values are given in [65].

With appropriate parameter values, the substrate and product levels of PFK oscillate. An example of these glycolytic oscillations is given in Fig. 10. The top panel shows the FBP time course, with a period of 7 min. When viewed in the F6P-FBP phase plane (bottom panel), the trajectory moves along a limit cycle (red). This encircles a single unstable node formed by the intersection of the F6P-nullcline (black dotted) and the FBP-nullcline (black solid). The latter has a cubic shape, and intersections that occur on the middle branch can correspond to unstable equilibria, as in this case. Intersections occurring on the upper or lower branches correspond to stable equilibria, and there are no oscillations. Changes in parameter values can move the nullclines so that intersections occur on any of the branches and thereby change stability of the equilibrium.

An important parameter in the system is the glucokinase flux rate, J_{GK}, which reflects the glucose concentration; higher glucose concentrations lead to higher values of J_{GK}. If J_{GK} is reduced to a sufficiently low level the system goes through a subcritical Hopf bifurcation and oscillations stop. If it is increased to a sufficiently high level then the system again goes through a subcritical Hopf bifurcation and oscillations stop. Thus, glycolytic oscillations only occur between lower and upper threshold values of J_{GK} [66].

Compound and accordion bursting

It is a long road from FBP production to ATP synthesis, involving the remainder of glycolysis, followed by the citric acid cycle, and ultimately oxidative phosphorylation where most of the ATP is produced. In the original DOM, this complexity is reduced to a single differential

equation, for the rate of change of the ADP concentration in the cytosol. This equation was derived by Keizer and Magnus in 1989 [9]:

$$\frac{d\mathrm{ADP}}{dt} = \frac{1}{\tau_a}\left[\mathrm{ATP} - \mathrm{ADP}\, e^{(r+\gamma)(1-c/r_1)}\right] \tag{21}$$

where the input from glycolysis comes through the term γ:

$$\gamma = \frac{v_\gamma J_{\mathrm{PDH}}}{k_\gamma + J_{\mathrm{PDH}}}\,. \tag{22}$$

In this way, an increase in FBP leads to a decrease in ADP, which has been converted to ATP. Another variable that enters the ADP differential equation is the cytosolic Ca^{2+}, c, reflecting the depolarizing effect that c influx into the mitochondria has on the mitochondrial membrane potential, reducing the driving force for ATP synthesis [9,67]. The cytosolic ATP concentration is then determined from the conservation of adenine nucleotides:

$$\mathrm{ATP} = A_{\mathrm{tot}} - \mathrm{AMP} - \mathrm{ADP} \tag{23}$$

where A_{tot} is the total adenine nucleotide concentration (a parameter), and AMP (adenosine monophosphate) is treated as in equilibrium with ATP and ADP:

$$\mathrm{AMP} = \frac{\mathrm{ADP}^2}{\mathrm{ATP}}\,. \tag{24}$$

(With this and the nucleotide conservation equation, Eq. (23), one only needs a single differential equation for nucleotides. In the Keizer-Magnus model, a differential equation for ADP was used, and this was retained in the IOM as Eq. (21).) Finally, the conductance of the K(ATP) current, $g_{\mathrm{K(ATP)}}$, is an increasing function of ADP and a decreasing function of ATP, given by the function o_∞(ADP,ATP). Then,

$$g_{\mathrm{K(ATP)}} = \bar{g}_{\mathrm{K(ATP)}} o_\infty(\mathrm{ADP}, \mathrm{ATP}). \tag{25}$$

The mathematical expression of o_∞ and other details including parameter values are described in the original DOM publication [32], and are not replicated here.

The differential equations in the DOM are all given above, but are gathered together here to aid readability:

$$\frac{dV}{dt} = -[I_{\mathrm{Ca}} + I_{\mathrm{K}} + I_{\mathrm{K(Ca)}} + I_{\mathrm{K(ATP)}}]/C_m \tag{26}$$

$$\frac{dn}{dt} = \frac{n_\infty(V) - n}{\tau_n} \tag{27}$$

$$\frac{dc}{dt} = f_c(J_{\mathrm{mem}} + J_{\mathrm{ER}}) \tag{28}$$

$$\frac{dc_{\mathrm{ER}}}{dt} = -f_{\mathrm{ER}}\sigma_v J_{\mathrm{ER}} \tag{29}$$

$$\frac{d\mathrm{F6P}}{dt} = 0.3(J_{\mathrm{GK}} - J_{\mathrm{PFK}}) \tag{30}$$

$$\frac{d\mathrm{FBP}}{dt} = J_{\mathrm{PFK}} - \frac{1}{2}J_{\mathrm{PDH}} \tag{31}$$

$$\frac{d\mathrm{ADP}}{dt} = \frac{1}{\tau_a}\left[\mathrm{ATP} - \mathrm{ADP}\, e^{(r+\gamma)(1-c/r_1)}\right]\,. \tag{32}$$

Depending on the parameter values, this model can produce a wide range of bursting patterns, including the fast and slow oscillations that the phantom burster can generate, but also the patterns that drove the development of the model, which are difficult if not impossible to explain without two oscillators. Fig. 11A shows compound bursting produced by the DOM, where there are episodes of bursts separated by long quiescent phases. Each episode is driven by a pulse of FBP (panel B), which leads to a pulse of ATP. These ATP pulses, generated through the glyoclytic oscillator, produce the burst episodes through their action on K(ATP) channels. In contrast, each burst in an episode is driven by oscillations in the K(Ca) conductance resulting from Ca^{2+} influx and subsequent removal, as described above for the phantom bursting model.

If the maximum K(ATP) conductance $g_{\mathrm{K(ATP)}}$ is reduced, accordion bursting is produced (Fig. 11C). In this case, rather than turning episodes on and off, the oscillations in K(ATP) conductance modulate

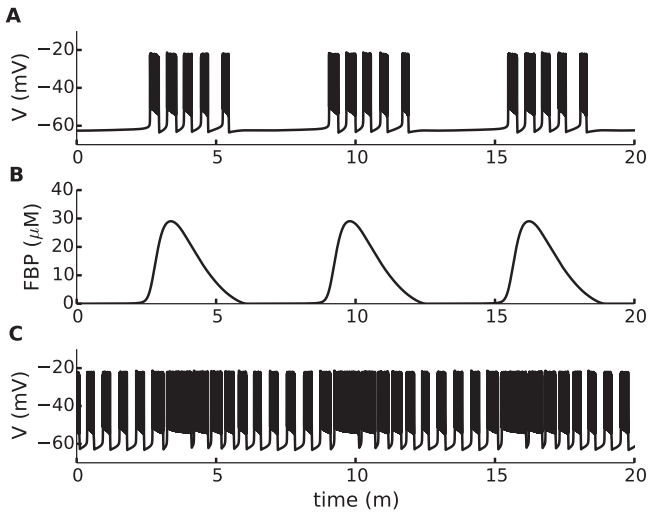

Fig. 11. Compound and accordion bursting produced by the DOM. **(A)** During compound bursting there are episodes of bursts followed by long periods of quiescence. **(B)** Intrinsic metabolic oscillations package the bursts into episodes. Each pulse of FBP produces an episode of bursts. **(C)** A reduction in the K(ATP) conductance converts compound bursting into accordion bursting, in which there is a slow rhythm in the burst plateau fraction.

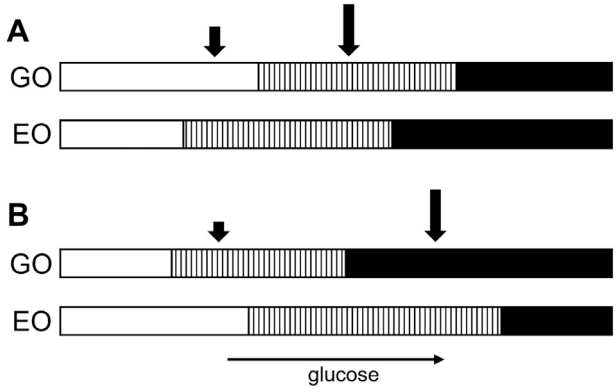

Fig. 12. (A) Illustration of the DOM. The top bar represents the glycolytic oscillator, while the bottom represents the electrical oscillator. Open sections indicate a low equilibrium state, hatched sections indicate an oscillatory state, and filled sections indicate a high equilibrium state. The small left arrow indicates a glucose level that produces fast bursting. The larger right arrow is a higher glucose level that produces slow bursting. Movement from one to the other, across the GO threshold, is a regime change as shown in Fig. 13. **(B)** The GO bar is left-shifted relative to the EO bar to illustrate the transitions that occur in Fig. 16 as the glucose level is slowly increased. The small leftmost arrow indicates a low glucose level, producing the subthreshold metabolic oscillations that occur during the first 30 min of Fig. 16. The large rightmost large arrow indicates a glucose level past the top threshold for the GO and producing the slow bursting with passive metabolic oscillations that occur during the last 20 min of Fig. 16.

the burst plateau fraction in a rhythmic manner. Importantly, the plateau fraction modulatory rhythm is periodic, as was reported in the experimental studies that quantified this burst pattern in islet β-cells [55,56].

Regime changes are predicted by the DOM

The name "Dual Oscillator Model" came from the coexistence of electrical and glycolytic oscillators in the model. The electrical oscillator produces fast bursting, while the glycolytic oscillator produces the slow rhythm underlying slow, compound, or accordion bursting. Each oscillator has lower and upper thresholds. Thus, a low glucose level could position the system below the lower threshold, while a high

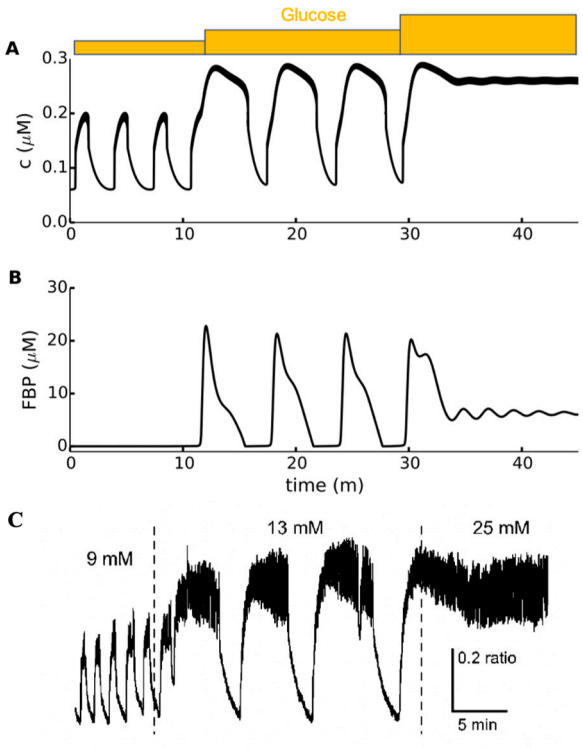

Fig. 13. Regime changes occur when the glucose concentration is increased. **(A, B)** At the first glucose level the electrical oscillator in the DOM is on and the glycolytic oscillator is off, so c oscillations are due to fast bursting. When glucose is increased past the upper threshold for the EO and lower threshold for the GO, much slower and larger c oscillations are produced, driven by the GO. When glucose is increased past the upper GO threshold, this slow oscillator turns off and the c concentration is tonically elevated while the membrane potential spikes continuously. **(C)** Experimental Ca^{2+} recording using the fluorescence dye fura-2. Regime changes occur when the glucose concentration is increased from 9 to 13 mM and later to 25 mM.
Source: This panel reproduced from [68].

level could position it above the upper threshold, and in either case there would be no oscillations. The oscillator is active only between the two thresholds. This is a very useful organizational structure that helps one interpret the DOM in an intuitive way. All the possible bursting behaviors can be understood by the ordering of the thresholds and where the glucose level is relative to the thresholds [68]. For example, it is possible for the glucose level to be above the lower threshold for the electrical oscillator, but below that for the glycolytic oscillator, with the result that the system produces fast bursting. It should then be possible to transition to slow bursting by raising the glucose level above the lower threshold for the glycolytic oscillator. This is illustrated in Fig. 12A. We call this transition from an electrical to a glycolytic oscillation a *regime change*. This is strong additional evidence for the coexistence of two oscillators in β-cells. Other behaviors can occur when the thresholds are in different relative locations, as in Fig. 12B.

Regime changes were first seen in [69], though not recognized as such, and later in experiments performed by the Satin lab. The DOM was used to explore conditions for which they could happen. An example of a regime change produced by the DOM is illustrated in Fig. 13A,B, which shows the intracellular Ca^{2+} concentration and FBP at three different glucose levels. At the initial glucose level (represented by the glucokinase parameter J_{GK}) the glycolytic oscillator is inactive; the FBP concentration is at a constant low level. The glucose concentration is increased at time t=10 min, putting it above the lower threshold for the glycolytic oscillator, so the glycolytic oscillator turns on, and each pulse of FBP produces a pulse of ATP that closes K(ATP) channels and triggers a pulse of electrical activity that ends following the FBP pulse. The result is a slow bursting pattern. Importantly, this new pattern is characterized by Ca^{2+} pulses that are both longer-lasting and greater in amplitude than the original fast bursting, so the insulin secretion would be much greater. Increasing the glucose concentration further, above the upper threshold for both oscillators, is another regime change and results in a continuous spiking pattern with elevated, but non-oscillatory FBP. (There are small transient oscillations in FBP since J_{GK} is near the upper threshold Hopf bifurcation.)

In the experimental studies of regime change in mouse islets, the fluorescent dye fura-2 was used to monitor the intracellular Ca^{2+} concentration of islet β-cells [68]. We found 11 examples of islets exhibiting regime changes when glucose was increased, one of which is shown in Fig. 13C. As shown in model simulations, the Ca^{2+} levels of the slow oscillations that occurred following the first increase in glucose were both wider and had greater amplitude than the oscillations prior to the regime change. This is a compelling example of how the underlying simplicity of the DOM, with two-semi-independent oscillators, facilitated our understanding of a behavior that would have been perplexing without the aid of the model.

This simple picture was soon challenged, however, by data from the Kennedy lab in which metabolic oscillations in islets were terminated when the cell membrane was hyperpolarized by the K(ATP) channel agonist diazoxide [70]. This was interpreted as indicating that metabolic oscillations are driven by the Ca^{2+} oscillations that occur when the cell is bursting with no need for a glycolytic oscillator. This had been proposed previously by Keizer and Magnus [9], who hypothesized that Ca^{2+} flux across the mitochondrial inner membrane depolarizes the membrane and thereby reduces ATP synthesis. This mechanism was incorporated into the phantom burster [4] and inherited by the DOM as Eq. (21), where it contributes to fast bursting when the glycolytic oscillator is not active. Another mechanism that can produce very similar results is the consumption of ATP by Ca^{2+}ATPase pumps that remove Ca^{2+} from the cytosol [71].

We showed that the DOM could provide an alternate explanation: membrane hyperpolarization closes Ca^{2+} channels, which lowers c. Because of this, the Ca^{2+} pumps are less active, so there is less ATP hydrolysis. Therefore, the ATP concentration rises and inhibits PFK, shutting off the glycolytic oscillations. The validity of this explanation was reinforced when we demonstrated that the metabolic oscillations could be recovered by depolarizing the cell with KCl in the presence of diazoxide [72]. This increases c, but without oscillations. Clearly then, metabolic oscillations can occur without Ca^{2+} oscillations. This result is not compatible with mechanisms in which metabolic oscillations occur only secondary to Ca^{2+} oscillations.

5. The integrated oscillator model

5.1. Measurement of FBP leads to more changes in the model

Another challenge arose later when our lab developed a FRET biosensor to detect oscillations in FBP, called PKAR (Pyruvate Kinase Activity Reporter) [74]. While use of the probe in islets clearly showed slow oscillations in PKAR (and thus FBP), the shape of the oscillations did not match those of the FBP oscillations in the DOM [73]. In particular, rather than the pulses of FBP shown in Figs. 11 and 13, the PKAR data indicated that FBP in islets has a sawtooth shape during bursting, declining during the active phase and rising during the silent phase (Fig. 14). This could not be explained by the DOM. The correct FBP pattern was achieved by including Ca^{2+}-dependent activation of pyruvate dehydrogenase (PDH) [75] into the model. This enzyme is downstream of PFK, and has been shown to be allosterically activated by Ca^{2+} [76]. In the model, then, we modified Eq. (20) to

$$J_{PDH} = v_{PDH} s_\infty(c_m)\sqrt{FBP/(1\mu M)} \tag{33}$$

where

$$s_\infty(c_m) = \frac{c_m}{K_{PDH} + c_m} \tag{34}$$

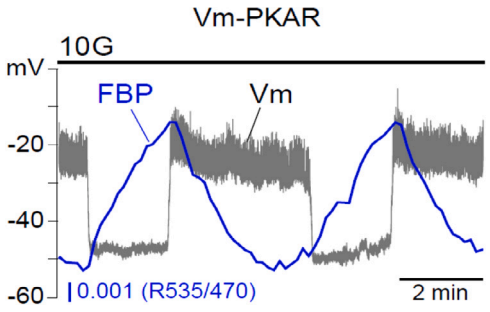

Fig. 14. Simultaneous recording of the membrane potential from a β-cell within an islet (Vm) in gray and fluorescence from the pyruvate kinase activity reporter (PKAR) in blue. PKAR is a Förster resonance energy transfer (FRET) biosensor that reports the FBP concentration in islet cells.
Source: Reproduced from [73].

and c_m is the free Ca^{2+} concentration in the mitochondria. This Ca^{2+} concentration is given by

$$\frac{dc_m}{dt} = f_c \sigma_m J_m \tag{35}$$

where J_m is the net Ca^{2+} flux into the mitochondria and the parameter σ_m is the ratio of cytosolic volume to mitochondrial volume. The flux term reflects Ca^{2+} pumping into the mitochondria by uniporters and efflux from mitochondria through Na^+-Ca^{2+} exchangers:

$$J_m = k_{uni} c - k_{NaCa}(c_m - c)\,. \tag{36}$$

The sawtooth shape of FBP, and specifically the decline of FBP during the active phase, comes about because high Ca^{2+} activates PDH, which draws FBP out of the cytosol into the mitochondria. This enhances ATP production in the mitochondria at the same time as it suppresses glycolytic oscillations by removing the positive feedback of FBP onto PFK.

With this addition to the model, the semi-independence of the electrical and metabolic oscillators was gone. Now, Ca^{2+} influences metabolism both through production and consumption of ATP, and ATP influences electrical activity and thus the Ca^{2+} concentrations through K(ATP) channels. In the revised model, Ca^{2+} can both stimulate PFK by increasing ATP consumption, which relieves the inhibition of PFK by ATP, and inhibit PFK by removing the stimulation of PFK by FBP. As a consequence, the two oscillators are closely and bidirectionally linked, motivating the name *Integrated Oscillator Model (IOM)* [34].

The IOM exhibits both passive and active metabolic oscillations

A key new feature of the IOM is that it possesses two co-existing mechanisms for slow metabolic oscillations. In one mechanism, metabolic oscillations are driven by oscillations in glycolysis, and are referred to as *active metabolic oscillations (AMOs)*. This is the type of metabolic oscillation that is responsible for slow, compound, and accordion bursting in the DOM. The other type of metabolic oscillation, *passive metabolic oscillations (PMOs)*, is due to the effects of Ca^{2+} on ATP consumption. With this mechanism, the Ca^{2+} concentration is elevated during a burst active phase, hydrolyzing ATP to power the Ca^{2+} pumps. When the ATP/ADP ratio drops to a sufficiently low level, the K(ATP) conductance becomes sufficiently large to turn off spiking and a silent phase begins. During this phase the Ca^{2+} concentration is low, reducing the ATP hydrolysis by pumps, causing the ATP/ADP ratio to build up and decreasing the K(ATP) conductance. Eventually, this conductance becomes small enough that spiking begins again, initiating a new burst active phase. Therefore, the Ca^{2+}-driven oscillations in ATP/ADP act very much as cytosolic Ca^{2+} did in the Chay–Keizer to drive bursting (in this case, slow bursting), but now through the K(ATP) current rather than the K(Ca) current. This is illustrated in Fig. 15,

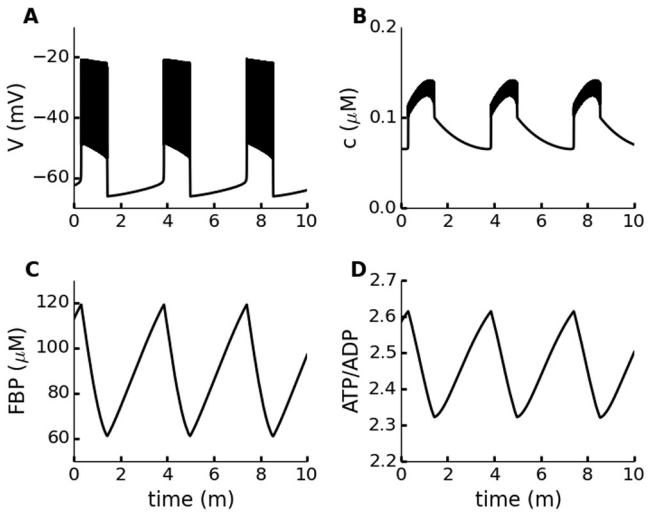

Fig. 15. Slow bursting with passive metabolic oscillations produced by the IOM. **(A, B)** Voltage and Ca^{2+} concentration profiles exhibit 4-min oscillations. These are the variables most readily measured in experiments. **(C)** The FBP level falls during a burst active phase and rises during a silent phase, as has been observed experimentally using the PKAR sensor [73]. **(D)** The ATP/ADP ratio has a sawtooth appearance, as has been observed experimentally using the fluorescent biosensor Perceval-HR [73,77,78].

where slow bursting with a period of approximately 4 min is shown. As in experiments using the PKAR FRET sensor to measure the FBP level, the FBP concentration declines during a burst active phase and rises during a silent phase (Fig. 14 and [73,74]). The ATP/ADP ratio, which sets the K(ATP) channel conductance, also has a sawtooth shape, as observed in experiments using the Perceval-HR biosensor to measure ATP/ADP [73,77,78].

The mechanism described above of PMO mode is very similar to the mechanism of slow oscillations in the phantom burster, and in fact, PMOs are a form of phantom bursting [79]. Thus, although the phantom mechanism appeared at first to be superseded by the glycolytic mechanism of the DOM, it was reborn in the IOM as a competitor to AMOs.

Since there are two mechanisms for metabolic oscillations in the IOM, it is natural to ask which occurs in the actual β-cells. There is compelling evidence that both do. In the experiments shown in [73–75], FBP and ATP/ADP levels had a sawtooth shape during slow bursting oscillations. This is an indicator of PMOs. However, metabolic oscillations have also been observed in situations in which the Ca^{2+} concentration was not oscillating [72,80], so the metabolic oscillations that occurred in these conditions must be AMOs. Also, we know of no other way to explain compound and accordion bursting [32,55,56] than as the electrical ramifications of AMOs acting on K(ATP) channels [32,65].

Why do beta cells have both AMOs and PMOs?

Another natural question is what benefit having two types of slow oscillations provides. A clue can be found by considering oscillations in basal (fasting) glucose.

All of the behaviors that we have discussed thus far occur when the glucose concentration is at a high enough level that the cell produces electrical activity. These are often referred to as *stimulatory glucose levels* since this is the case when the insulin secretion is greatest. However, insulin is also secreted when the glucose level is low, at fasting levels below the threshold for electrical activity. With these *basal glucose levels* the insulin secretion is much less, but measurements made in vivo at basal glucose levels from monkeys [81], humans [82,83], and dogs [84] and in isolated islets from *ob/ob* mice [85] and humans [86]

show pulsatility in the insulin level with the same period as the large amplitude pulses in high glucose. We have hypothesized that Ca^{2+} does not rise high enough in basal glucose to drive oscillations by feedback on any ion channels and that therefore the insulin secretion oscillations are due to AMOs [87]. Under this scenario, the metabolic oscillations cause pulsatile insulin secretion by modulating the trafficking of insulin vesicles to the plasma membrane. The secretion is at a low level since the Ca^{2+} concentration in the cell is low, but plausibly it can still oscillate by this mechanism. Metabolic modulation of insulin secretion is well established in stimulatory glucose, where it accounts for about half of insulin secretion, and is called the glucose amplification factor [88,89]. The hypothesis that it underlies basal secretion oscillations remains to be tested.

The numerical simulation with the IOM in Fig. 16 illustrates a way in which AMOs and PMOs could work together, with AMOs providing secretion oscillations in basal glucose, and PMOs taking over in stimulatory glucose. The glucose concentration is initially held constant at a basal level of 3 mM, during which AMOs are generated. These are characterized by pulses of FBP and ATP/ADP and small oscillations in the membrane potential that occur due to the actions of ATP/ADP on current through K(ATP) channels. As the glucose concentration is slowly ramped up the model cell begins to burst. These bursts are driven by PMOs, characterized by sawtooth time courses in FBP and ATP/ADP. The switch to PMOs is needed here because the AMOs are prevented by a combination of high glucose carrying the glycolytic oscillator across its upper threshold and by PDH channeling Ca^{2+} away from PFK into the mitochondria. With the two oscillator modes working together, there would be pulsatile insulin secretion due to the oscillations over the entire physiological range of glucose due to metabolism acting on the glucose amplification factor. The insulin pulses would be of much larger amplitude once bursting commences since the Ca^{2+} concentration would be elevated during each burst and trigger exocytosis of insulin-containing granules.

The scenario above is an example of one of the many possible behaviors that can occur when the GO and EO thresholds are in different locations relative to one another. In the case of Fig. 16, the GO bottom threshold is at a lower glucose level than the bottom threshold for the EO (Fig. 12B), so oscillations in metabolism are possible at a low level of glucose (leftmost arrow). The higher glucose level that produces bursting is above the top threshold for the GO, but still below the top threshold for the EO (rightmost arrow). The result is slow bursting with sawtooth patterns in the FBP and ATP/ADP time courses, characteristic of PMOs (Fig. 16).

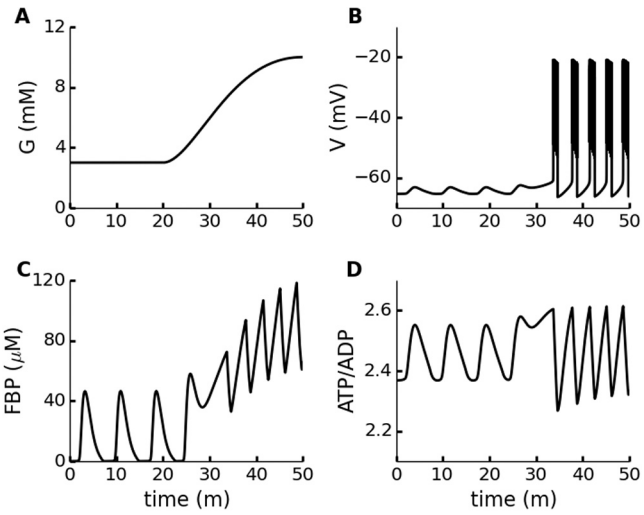

Fig. 16. Ramping from basal to stimulatory glucose levels converts AMOs to PMOs. **(A)** The glucose concentration begins at a steady basal level and is then ramped up to stimulatory values. **(B)** The voltage initially exhibits small subthreshold oscillations, and later switches to slow bursting when the K(ATP) conductance is sufficiently small. **(C)** The FBP time course is pulsatile when glucose is at a substimulatory level and later has a sawtooth shape at stimulatory glucose levels. **(D)** The ATP/ADP ratio has a pulsatile appearance when the metabolic oscillations are active, and a sawtooth appearance when they are passive.

6. Chay-Keizer looks at 40

In the 40 years since its publication, the Chay–Keizer model has had an outsized impact on the field of islet biology. As a model for bursting in β-cells it is incomplete, but it correctly identifies the driving mechanism of activity-dependent Ca^{2+} feedback via K(Ca) ion channels. In addition to the IOM and models leading up to it, the Chay–Keizer model spawned a host of other models postulating different negative feedback variables. These include Ca^{2+}-dependent inactivation of an inward current [90], Ca^{2+} inhibition of oxidative phosphorylation and its effect on ATP synthesis, which affects K(ATP) channels [9,42,67], voltage-dependent inactivation of Ca^{2+} channels [10], the slow variation of the ER-Ca^{2+} concentration acting on the membrane through its effect on cytosolic Ca^{2+} and K(Ca) channels [6] or store operated inward current (SOC) [91], the slow variation of intracellular Na^+ and the consequent activation of the electrogenic Na^+-K^+ exchanger [7], hydrolysis of ATP by Ca^{2+} pumps and the subsequent decline in ATP/ADP that opens K(ATP) channels [44,71], or a combination of mechanisms including K(ATP) channels and electrogenic transporter currents at different glucose levels [5]. Only the hypothesis of Tornheim, that there is an endogenous glycolytic oscillator underlying bursting [64], broke entirely from the Chay–Keizer mold. The DOM and IOM combined the idea of Ca^{2+}-dependent inhibition with an endogenous glycolytic oscillator, and so built on pioneering work from both Chay–Keizer and Tornheim.

Amidst all this exploration of alternative negative feedback mechanisms, the Chay–Keizer paradigm, first explicated by Rinzel, in which square-wave bursting arises from bistability between silent and spiking states has shown remarkable durability. We suspect that this is really how it works and is not just lack of imagination on the part of theorists because other burst patterns that look similar in several pituitary cell types appear not to involve bistability and have different predicted mathematical properties [92,93]. Some of these predictions have been tested experimentally [94], and some remain to be tested.

The main revisions to the paradigm have been the realization that accounting for the diversity of oscillation patterns exhibited by β-cells requires additional mechanisms. Two or more slow variables (phantom bursting) are needed to give a wide range of periods. Two other current models that can produce a wide range of periods also turn out to be phantom bursters [5,7]. To account for compound and subthreshold oscillations, a second oscillator has to be added (DOM or IOM).

This leaves us with the question, why does it have to be so complicated? We have proposed that two kinds of slow oscillations (AMOs and PMOs) are needed to seamlessly coordinate pulsatile insulin secretion in basal and stimulatory glucose [87]. This prediction needs to be tested experimentally, and we have begun to do so. This is the apotheosis of the unification of Chay–Keizer and Tornheim. Pure ionic models cannot produce oscillations in basal glucose, and pure metabolic models can only produce minuscule oscillations of calcium unless the threshold for electrical bursting is crossed.

The slow electrical oscillations have clear physiological relevance because they drive pulsatile insulin secretion, which enhances the efficacy of insulin on its target tissues, but the role of the fast oscillations is less obvious. We conjecture that they are part of the modulation of beta-cell electrical activity by neuronal and hormonal signals (such as acetylcholine and glucagon-like peptide 1), which act on small ionic currents and the ER to increase oscillation frequency and raise mean calcium. This is also where the K(Ca) channel, otherwise dispensable, takes center stage. The prototype example of this is a model of the

effects of acetylcholine [95], which we realized only years later was a phantom burster.

The Chay–Keizer model has also been the focus of developments aimed at understanding the different forms of bursting from a purely mathematical perspective. It was one of the models used in the pioneering fast/slow analysis of bursting [15,22,23] and has continued to be employed in mathematical studies of bursting [96–98].

The discussion of β-cell models in this article assumes that all β-cells in the islet are in synchrony, so that the model describes a representative cell in a synchronized population of cells. This approximation is both useful and valid for most questions regarding islet activity; synchrony is produced through gap junctions that provide electrical coupling among β-cells, and Ca^{2+} measurements from different regions of an islet showed synchronized oscillations [27]. However, more recent studies showed the presence of Ca^{2+} waves across an islet [99,100], demonstrating some degree of spatial nonuniformity of activity on a shorter time scale. Also, there has been recent experimental work indicating the presence of islet "hub cells" that play an outsized role in the generation of bursting activity across the islet [101], but this remains a topic of debate that some argue against [102–104]. Another interesting question is that of how the hundreds of thousands of islet oscillators within a pancreas are coordinated, a question that has been the focus of some mathematical model work [105] and in vitro testing of hypotheses [106–109]. Finally, the Chay–Keizer model and the IOM are models for β-cells in mouse islets, where most of the experimental data exists. Some modeling work has also been done for human islets [11,12,110], which have some different ionic currents and potentially different burst mechanisms.

Looking back over 40 years, then, it is evident that the Chay–Keizer model has had a lasting influence on the way that the scientific community understands bursting oscillations, and opened the door for further exploration of the burst mechanism in pancreatic β-cells. The IOM is the most advanced descendent, having been developed over more than two decades of iteration between experimental and mathematical developments. The authors hope that further developments to the IOM will continue into the future, further extending the legacy of the Chay–Keizer model.

Funding

RB was partially supported by National Science Foundation, United States Grant DMS 2324962. L.S.S. was partially supported by National Institute of Diabetes and Digestive and Kidney Diseases (NIDDK), United States Grants RO1 DK46409 and U01 DK127747. P.A.F. and A.S.S. were supported by the Intramural Research Program of the NIDDK, United States under ZIA DK013027. I.M. acknowledges financial support from the University of Birmingham Dynamic Investment Fund, United Kingdom.

Declaration of competing interest

None.

References

[1] T.R. Chay, J. Keizer, Minimal model for membrane oscillations in the pancreatic β-cell, Biophys. J. 42 (1983) 181–190.
[2] I. Atwater, C.M. Dawson, A. Scott, G. Eddlestone, E. Rojas, The nature of the oscillatory behavior in electrical activity for pancreatic β-cell, in: G. Thieme (Ed.), Biochemistry and Biophysics of the Pancreatic β-Cell, Verlag, New York, 1980, pp. 100–107.
[3] T.R. Chay, J. Rinzel, Bursting, beating, and chaos in an excitable membrane model, Biophys. J. 47 (1985) 357–366.
[4] R. Bertram, A. Sherman, A calcium-based phantom bursting model for pancreatic islets, Bull. Math. Biol. 66 (2004) 1313–1344.
[5] C.Y. Cha, Y. Nakamura, Y. Himeno, J. Wang, S. Fujimoto, N. Inagaki, Y.E. Earm, A. Noma, Ionic mechanisms and Ca^{2+} dynamics underlying the glucose response of pancreatic β cells, Am. J. Physiol. 138 (2011) 21–37.
[6] T.R. Chay, Electrical bursting and luminal calcium oscillation in excitable cell models, Biol. Cybernet. 75 (1996) 419–431.
[7] L.E. Fridlyand, N. Tamarina, L.H. Philipson, Modeling of Ca^{2+} flux in pancreatic β-cells: role of the plasma membrane and intracellular stores, Am. J. Physiol. 285 (2003) E138–E154.
[8] L.E. Fridlyand, D.A. Jacobson, A. Kuznetsov, L.H. Philipson, A model of action potentials and fast Ca^{2+} dynamics in pancreatic β-cells, Biophys. J. 2009 (2009) 3126–3139.
[9] J. Keizer, G. Magnus, ATP-sensitive potassium channel and bursting in the pancreatic β cell, Biophys. J. 56 (1989) 229–242.
[10] J. Keizer, P. Smolen, Bursting electrical activity in pancreatic β cells caused by Ca^{2+}- and voltage-inactivated Ca^{2+} channels, Proc. Natl. Acad. Sci. 88 (1991) 3897–3901.
[11] M.G. Pedersen, A biophysical model of electrical activity in human β-cells, Biophys. J. 99 (2010) 3200–3207.
[12] M. Riz, M. Braun, M.G. Pedersen, Mathematical modeling of heterogeneous electrophysiological responses in human β-cells, PLoS Comp. Biol. 20 (1) (2014) e1003389.
[13] A. Sherman, J. Keizer, J. Rinzel, Domain model for Ca^{2+}-inactivation Ca^{2+} channels at low channel density, Biophys. J. 58 (1990) 985–995.
[14] G.J. Félix-Martínez, J.R. Godínez-Fernández, A primer on modelling pancreatic islets: from models of coupled β-cells to multicellular islet models, Islets 15:1 (2023) 2231609.
[15] J. Rinzel, Y.S. Lee, On different mechanisms for membrane potential bursting, in: H.G. Othmer (Ed.), Nonlinear Oscillations in Biology and Chemistry, in: Lecture Notes in Biomathematics, vol. 66, Springer–Verlag, Berlin, 1985, pp. 19–33.
[16] E. Av-Ron, H. Parnas, L. Segel, A basic biophysical model for bursting neurons, Biol. Cybernet. 69 (1993) 87–95.
[17] E. Barreto, J.R. Cressman, Ion concentration dynamics as a mechanism for neuronal bursting, J. Biol. Phys. 37 (2011) 361–373.
[18] R. Barrio, A. Shilnilkov, Parameter-sweeping techniques for temporal dynamics of neuronal systems:case study of hindmarsh-rose model, J. Math. Neurosci. 1 (6) (2011) http://dx.doi.org/10.1186/2190--8567--1--6.
[19] R. Bertram, M.J. Butte, T. Kiemel, A. Sherman, Topological and phenomenological classification of bursting oscillations, Bull. Math. Biol. 57 (1995) 413–439.
[20] J. Best, A. Borisyuk, J. Rubin, D. Terman, M. Wechselberger, The dynamic range of bursting in a model respiratory pacemaker network, SIAM J. Appl. Dyn. Sys. 4 (2005) 1107–1139.
[21] E.M. Izhikevich, Neural excitability, spiking, and bursting, Int. J. Bifurcation Chaos 10 (2000) 1171–1266.
[22] J. Rinzel, A formal classification of bursting mechanisms in excitable systems, in: E. Teramoto, M. Yamaguti (Eds.), Mathematical Topics in Population Biology, Morphogenesis and Neurosciences, in: Lecture Notes in Biomathematics, vol. 71, Springer, Berlin, 1987, pp. 267–281.
[23] J. Rinzel, Y.S. Lee, Dissection of a model for neuronal parabolic bursting, J. Math. Biol. 25 (1987) 653–675.
[24] A. Sherman, Anti-phase, asymmetric, and aperiodic oscillations in electrically active cells I. Coupled bursters, Bull. Math. Biol. 56 (1994) 811–835.
[25] R. Bertram, J. Rubin, Multi-timescale systems and fast-slow analysis, Math. Biosci. 287 (2017) 105–121.
[26] P.M. Dean, E.K. Mathews, Glucose-induced electrical activity in pancreatic islet cells, J. Physiol. 210 (1970) 255–264.
[27] R.M. Santos, L.M. Rosario, A. Nadal, J. Garcia-Sancho, B. Soria, M. Valdeolmillos, Widespread synchronous $[Ca^{2+}]_i$ oscillations due to bursting electrical activity in single pancreatic islets, Pflügers Arch. 418 (1991) 417–422.
[28] M. Zhang, P. Goforth, R. Bertram, A. Sherman, L. Satin, The Ca^{2+} dynamics of isolated mouse β-cells and islets: Implications for mathematical models, Biophys. J. 84 (2003) 2852–2870.
[29] C.S. Nunemaker, M. Zhang, D. Wasserman, O.P. McGuinness, A.C. Powers, R. Bertram, A. Sherman, L.S. Satin, Individual mice can be distinguished by the period of their islet calcium oscillations: Is there an intrinsic islet period that is imprinted in vivo? Diabetes 54 (2005) 3517–3522.
[30] M. Valdeolmillos, R.M. Santos, D. Contreras, B. Soria, L.M. Rosario, Glucose-induced oscillations of intracellular Ca^{2+} concentration resembling bursting electrical activity in single mouse islets of langerhans, FEBS Lett. 259 (1989) 19–23.
[31] P. Krippeit-Drews, M. Düfer, G. Drews, Parallel oscillations of intracellular calcium activity and mitochondrial membrane potential in mouse pancreatic β-cells, Biochem. Biophys. Res. Comm. 267 (2000) 179–183.
[32] R. Bertram, L. Satin, M. Zhang, P. Smolen, A. Sherman, Calcium and glycolysis mediate multiple bursting modes in pancreatic islets, Biophys. J. 87 (2004) 3074–3087.
[33] R. Bertram, A. Sherman, L.S. Satin, Metabolic and electrical oscillations: Partners in controlling pulsatile insulin secretion, Am. J. Physiol. 293 (2007) E890–E900.
[34] R. Bertram, L.S. Satin, A.S. Sherman, Closing in on the mechanisms of pulsatile insulin secretion, Diabetes 67 (2018) 351–359.

[35] A.L. Hodgkin, A.F. Huxley, A quantitative description of membrane current and its application to conduction and excitation in nerve, J. Physiol. 117 (1952) 500–544.

[36] F.M. Ashcroft, D.E. Harrison, S.J.H. Ashcroft, Glucose induces closure of single potassium channels in isolated rat pancreatic β-cells, Nature 312 (1984) 446–448.

[37] D.L. Cook, C.N. Hales, Intracellular ATP directly blocks K^+ channels in pancreatic B-cells, Nature 311 (1984) 271–273.

[38] F.M. Ashcroft, P. Rorsman, K_{ATP} channels and islet hormone secretion: new insights and controversies, Nature Rev. 9 (2013) 660–669.

[39] J. Rinzel, G.B. Ermentrout, Analysis of neural excitability and oscillations, in: C. Koch, I. Segev (Eds.), Methods in Neuronal Modeling: From Synapses to Networks, Vol. 2, MIT Press, Cambridge, 1998, pp. 251–292.

[40] D.L. Cook, W.E. Crill, D. Porte, Jr., Glucose and acetylcholine have different effects on the plateau pacemaker of pancreatic islet cells, Diabetes 30 (1981) 558–561.

[41] D. Terman, The transition from bursting to continuous spiking in excitable membrane models, J. Nonlinear Sci. 2 (1992) 135–182.

[42] P. Smolen, J. Keizer, Slow voltage inactivation of Ca^{2+} currents and bursting mechanisms for the mouse pancreatic β-cell, J. Membrane Biol. 127 (1992) 9–19.

[43] L.E. Fridlyand, L.H. Philipson, Oxidative reactive species in cell injury: Mechanisms in diabetes mellitus and therapeutic approaches, Ann. New York Acad. Sci. 1066 (2005) 136–151.

[44] Y. Miwa, Y. Imai, Simulation of spike-burst generation and Ca^{2+} oscillations in pancreatic β-cells, Jpn. J. Physiol. 49 (1999) 353–364.

[45] M.A. Ravier, D. Daro, L.P. Roma, J.-C. Jonas, R. Cheng-Xue, F.C. Schuit, P. Gilon, Mechanisms of control of the free Ca^{2+} concentration in the endoplasmic reticulum of mouse pancreatic β-cells, Diabetes 60 (2011) 2533–2545.

[46] R. Bertram, J. Previte, A. Sherman, T.A. Kinard, L.S. Satin, The phantom burster model for pancreatic β-cells, Biophys. J. 79 (2000) 2880–2892.

[47] T.A. Kinard, G. de Vries, A. Sherman, L.S. Satin, Modulation of the bursting properties of single mouse pancreatic β-cells by artificial conductances, Biophys. J. 76 (1999) 1423–1435.

[48] P.A. Smith, F.M. Ashcroft, P. Rorsman, Simultaneous recordings of glucose dependent electrical activity and ATP-regulated K^+-currents in isolated mouse pancreatic β-cells, FEBS Lett. 261 (1990) 187–190.

[49] O. Larsson, H. Kindmark, R. Bränström, B. Fredholm, P.-O. Berggren, Oscillations in K_{ATP} channel activity promote oscillations in cytoplasmic free Ca^{2+} concentration in the pancreatic β cell, Proc. Natl. Acad. Sci. 93 (1996) 5161–5165.

[50] A. Sherman, J. Rinzel, J. Keizer, Emergence of organized bursting in clusters of pancreatic β-cells by channel sharing, Biophys. J. 54 (1988) 411–425.

[51] M.G. Pedersen, Phantom bursting is highly sensitive to noise and unlikely to account for slow bursting in β-cells: Considerations in favor of metabolically driven oscillations, J. Theoret. Biol. 248 (2007) 391–400.

[52] P. Smolen, J. Rinzel, A. Sherman, Why pancreatic islets burst but single β-cells do not: the heterogeneity hypothesis, Biophys. J. 64 (1993a) 1668–1679.

[53] A.A. Sharp, M.B. O'Neil, L.F. Abbott, E. Marder, The dynamic clamp: Artificial conductances in biological neurons, TINS 16 (1993) 389–394.

[54] J. Sánchez-Andrés, A. Gomis, M. Valdeolmillos, The electrical activity of mouse pancreatic β-cells recorded in vivo shows glucose-dependent oscillations, J. Physiol. 486 (1995) 223–228.

[55] J.C. Henquin, H.P. Meissner, W. Schmeer, Cyclic variations of glucose-induced electrical activity in pancreatic β cells, Pflügers Arch. 393 (1982) 322–327.

[56] D.L. Cook, Isolated islets of langerhans have slow oscillations of electrical activity, Metabolism 32 (1983) 681–685.

[57] R.M. Barbosa, A.M. Silva, A.R. Tomé, J.A. Stamford, R.M. Santos, L.M. Rosário, Control of pulsatile 5-HT/insulin secretion from single mouse pancreatic islets by intracellular calcium dynamics, J. Physiol. 510 (1998) 135–143.

[58] M.C. Beauvois, C. Merezak, J.-C. Jonas, M.A. Ravier, J.-C. Henquin, P. Gilon, Glucose-induced mixed $[Ca^{2+}]_c$ oscillations in mouse β-cells are controlled by the membrane potential and the SERCA3 Ca^{2+}-ATPase of the endoplasmic reticulum, Am. J. Physiol. 290 (2006) C1503–C1511.

[59] I. Marinelli, V. Parekh, P. Fletcher, B. Thompson, J. Ren, X. Tang, T.L. Saunders, J. Ha, A. Sherman, R. Bertram, L.S. Satin, Slow oscillations persist in pancreatic beta cells lacking phosphofructokinase m, Biophys. J. 121 (2022) 692–704.

[60] P. Bergsten, Slow and fast oscillations of cytoplasmic Ca^{2+} in pancreatic islets correspond to pulsatile insulin release, Am. J. Physiol. 268 (1995) E282–E287.

[61] L.S. Satin, P.C. Butler, J. Ha, A.S. Sherman, Pulsatile insulin secretion, impaired glucose tolerance and type 2 diabetes, Mol. Aspects Med. 42 (2015) 61–77.

[62] P. Smolen, A model for glycolytic oscillations based on skeletal muscle phosphofructokinase kinetics, J. Theoret. Biol. 174 (1995) 137–148.

[63] G.C. Yaney, V. Schultz, B.A. Cunningham, G.A. Dunaway, B.E. Corkey, K. Tornheim, Phosphofructokinase isozymes in pancreatic islets and clonal β-cells (INS-1), Diabetes 44 (1995) 1285–1289.

[64] K. Tornheim, Are metabolic oscillations responsible for normal oscillatory secretion? Diabetes 46 (1997) 1375–1380.

[65] I. Marinelli, T. Vo, L. Gerardo-Giorda, R. Bertram, Transitions between bursting modes in the integrated oscillator model for pancreatic β-cells, J. Theoret. Biol. 454 (2018) 310–319.

[66] M. Watts, B. Fendler, M.J. Merrins, L.S. Satin, R. Bertram, A. Sherman, Calcium and metabolic oscillations in pancreatic islets: Who's driving the bus? SIAM J. Appl. Dyn. Sys. 13 (2016) 683–703.

[67] G. Magnus, J. Keizer, Model of β-cell mitochondrial calcium handling and electrical activity. I. Cytoplasmic variables, Am. J. Physiol. 274 (1998) C1158–C1173.

[68] C.S. Nunemaker, R. Bertram, A. Sherman, K. Tsaneva-Atanasova, C.R. Daniel, L.S. Satin, Glucose modulates $[Ca^{2+}]$ oscillations in pancreatic islets via ionic and glycolytic mechanisms, Biophys. J. 91 (2006) 2082–2096.

[69] C.M. Antunes, A.P. Salgado, L.M. Rosário, R.M. Santos, Differential patterns of glucose-induced electrical activity and intracellular calcium responses in single mouse and rat pancreatic islets, Diabetes 49 (2000) 2028–2038.

[70] R.T. Kennedy, L.M. Kauri, G.M. Dahlgren, S.-K. Jung, Metabolic oscillations in β-cells, Diabetes 51 (2002) S152–S161.

[71] P. Detimary, P. Gilon, J.-C. Henquin, Interplay between cytoplasmic Ca^{2+} and the ATP/ADP ratio: A feedback control mechanism in mouse pancreatic islets, Biochem. J. 333 (1998) 269–274.

[72] M.J. Merrins, B. Fendler, M. Zhang, A. Sherman, R.. Bertram, L.S. Satin, Metabolic oscillations in pancreatic islets depend on the intracellular Ca^{2+} level but not Ca^{2+} oscillations, Biophys. J. 99 (2010) 76–84.

[73] M.J. Merrins, C. Poudel, J.P. McKenna, J. Ha, A. Sherman, R. Bertram, L.S. Satin, Phase analysis of metabolic oscillations and membrane potential in pancreatic β-cells, Biophys. J. 110 (2016) 691–699.

[74] M.J. Merrins, A.R.V. Dyke, A.K. Mapp, M.A. Rizzo, L.S. Satin, Direct measurements of oscillatory glycolysis in pancreatic islet β-cells using novel FRET biosensors for pyruvate kinase M2 activity, J. Biol. Chem. 288 (2013) 33312–33322.

[75] J.P. McKenna, J. Ha, M.J. Merrins, L.S. Satin, A. Sherman, R. Bertram, Ca^{2+} effects on ATP production and consumption have regulatory roles on oscillatory islet activity, Biophys. J. 110 (2016) 733–742.

[76] R.M. Denton, Regulation of mitochondrial dehydrogenases by calcium ions, Biochim. Biophys. Acta 1787 (2009) 1309–1316.

[77] J. Li, H.Y. Shuai, E. Gylfe, A. Tengholm, Oscillations of sub-membrane ATP in glucose-stimulated beta cells depend on negative feedback from Ca^{2+}, Diabetologia 56 (2013) 1577–1586.

[78] I. Marinelli, B.M. Thompson, V.S. Parekh, P.A. Fletcher, L. Gerardo-Giorda, A.S. Sherman, L.S. Satin, R. Bertram, Oscillations in K(ATP) conductance drive slow calcium oscillations in pancreatic β-cells, Biophys. J. 121 (2022) 1449–1464.

[79] J.P. McKenna, R. Bertram, Fast-slow analysis of the integrated oscillator model for pancreatic β-cells, J. Theoret. Biol. 457 (2018) 152–162.

[80] J. Ren, A. Sherman, R. Bertram, P.B. Goforth, C.S. Nunemaker, C.D. Waters, L.S. Satin, Slow oscillations in KATP conductance in mouse pancreatic islets provide support for electrical bursting driven by metabolic oscillations, Am. J. Physiol. 305 (2013) E805–E817.

[81] C.J. Goodner, B.C. Walike, D.J. Koerker, J.W. Ensinck, A.C. Brown, E.W. Chideckel, J. Palmer, L. Kalnasy, Insulin, glucagon, and glucose exhibit synchronous, sustained oscillations in fasting monkeys, Science 195 (1977) 177–179.

[82] D.A. Lang, D.R. Matthews, J. Peto, R.C. Turner, Cyclic oscillations of basal plasma glucose and insulin concentrations in human beings, N. Engl. J. Med. 301 (1979) 1023–1027.

[83] S.H. Song, S.S. McIntyre, H. Shah, J.D. Veldhuis, P.C. Hayes, P.C. Butler, Direct measurement of pulsatile insulin secretion from the portal vein in human subjects, J. Clin. Endocrinol. Metab. 85 (2000) 4491–4499.

[84] N. Pørksen, S. Munn, J. Steers, J.D. Veldhuis, P.C. Butler, Effects of glucose ingestion versus infusion on pulsatile insulin secretion, Diabetes 45 (1996) 1317–1323.

[85] J. Westerlund, P. Bergsten, Glucose metabolism and pulsatile insulin release from isolated islets, Diabetes 50 (2001) 1785–1790.

[86] R.A. Ritzel, J.D. Veldhuis, P.C. Butler, Glucose stimulates pulsatile insulin secretion from human pancreatic islets by increasing secretory burst massl dose-response relationships, J. Clin. Endocrinol. Metab. 88 (2003) 742–747.

[87] P.A. Fletcher, I. Marinelli, R. Bertram, L.S. Satin, A.S. Sherman, Pulsatile basal insulin secretion is driven by glycolytic oscillations, Physiology 37 (2022) http://dx.doi.org/10.1152/physiol.00044.2021.

[88] J.C. Henquin, Triggering and amplifying pathways of regulation of insulin secretion by glucose, Diabetes 49 (2000) 1751–1760.

[89] I. Rustenbeck, T. Schulze, M. Morsi, M. Alshafei, U. Panten, What is the metabolic amplification of insulin secretion and is it (still) relevant? Metabolites 11 (2021).

[90] T.R. Chay, D.L. Cook, Endogenous bursting patterns in excitable cells, Math. Biosci. 90 (1988) 139–153.

[91] M.W. Roe, J.F. Worley III, F. Qian, N. Tamarina, A.A. Mittal, F. Dralyuk, N.T. Blair, R.J. Mertz, L.H. Philipson, I.D. Dukes, Characterization of a Ca^{2+} release-activated nonselective cation current regulating membrane potential and $[Ca^{2+}]_i$ oscillations in transgenically derived β-cells, J. Biol. Chem. 273 (1998) 10402–10410.

[92] J.V. Stern, H.M. Osinga, A. LeBeau, A. Sherman, Resetting behavior in a model of bursting in secretory pituitary cells: Distinguishing plateaus from pseudo-plateaus, Bull. Math. Biol. 70 (2008) 68–88.

[93] T. Vo, R. Bertram, J. Tabak, M. Wechselberger, Mixed mode oscillations as a mechanism for pseudo-plateau bursting, J. Comput. Neurosci. 28 (2010) 443–458.
[94] T. Vo, J. Tabak, R. Bertram, M. Wechselberger, A geometric understanding of how fast activating potassium channels promote bursting in pituitary cells, J. Comput. Neurosci. 36 (2014) 259–278.
[95] R. Bertram, P. Smolen, A. Sherman, D. Mears, I. Atwater, F. Martin, B. Soria, A role for calcium release-activated current (CRAC) in cholinergic modulation of electrical activity in pancreatic β-cells, Biophys. J. 68 (1995) 2323–2332.
[96] W. Teka, K. Tsaneva-Atanasova, R. Bertram, J. Tabak, From plateau to pseudo-plateau bursting: Making the transition, Bull. Math. Biol. 73 (2011) 1292–1311.
[97] H.M. Osinga, A. Sherman, K.T. Tsaneva-Atanasova, Cross-currents between biology and mathematics: The codimension of pseudo-plateau bursting, Discrete Contin. Dyn. Syst. 32 (2012) 2853–2877.
[98] S.R. John, B. Krauskopf, H.M. Osinga, J.E. Rubin, Slow negative feedback enhances robustness of square-wave bursting, J. Comput. Neurosci. (2023) http://dx.doi.org/10.1007/s10827--023--00846--y.
[99] R.K.P. Benninger, M. Zhang, W.S. Head, L.S. Satin, D.W. Piston, Gap junction coupling and calcium waves in the pancreatic islet, Biophys. J. 95 (2008) 5048–5061.
[100] R.K.P. Benninger, T. Hutchens, W.S. Head, M.J.M. Caughey, M. Zhang, S.J. LeMarchand, L.S. Satin, D.W. Piston, Intrinsic islet heterogeneity and gap junction coupling determine spatiotemporal Ca^{2+} wave dynamics, Biophys. J. 107 (2014) 2723–2733.
[101] N.R. Johnston, R.K. Mitchell, E. Haythorne, M.P. Pessoa, F. Semplici, J. Ferrer, L. Plemonti, P. Marchetti, M. Bugliani, D. Bosco, E. Berishvili, P. Duncanson, M. Watkinson, J. Broichhagen, D. Trauner, G.A. Rutter, D.J. Hodson, Beta cell hubs dictate pancreatic islet responses to glucose, Cell Metab. 24 (2016) 389–401.
[102] J.M. Dwulet, J.K. Briggs, R.K.P. Benninger, Small subpopulations of β-cells do not drive islet oscillatory $[Ca^{2+}]$ dynamics via gap junction communication, PLoS Comput. Biol. 17 (2021) e1008948.
[103] B.E. Peercy, A.S. Sherman, Do oscillations in pancreatic islets require pacemaker cells? J. Biosci. 47 (2022) http://dx.doi.org/10.1007/s12038--021--00251--6.
[104] L.S. Satin, Q. Zhang, P. Rorsman, Take me to your leader: An electrophysiological appraisal of the role of hub cells in pancreatic islets, Diabetes 69 (2020) 830–836.
[105] M.G. Pedersen, R. Bertram, A. Sherman, Intra- and inter-islet synchronization of metabolically driven insulin secretion, Biophys. J. 89 (2005) 107–119.
[106] J.E. Adablah, R. Vinson, M.G. Roper, R. Bertram, Synchronization of pancreatic islets by periodic or non-periodic muscarinic agonist pulses, PLoS One 14 (2019) e0211832.
[107] N. Bruce, I.-A. Wei, W. Leng, Y. Oh, Y.-C. Chiu, M.G. Roper, R. Bertram, Coordination of pancreatic islet rhythmic activity by delayed negative feedback, Am. J. Physiol. 323 (2022) E492–E502.
[108] R. Dhumpa, T.M. Truong, X. Wang, R. Bertram, M.G.. Roper, Negative feedback synchronizes islets of langerhans, Biophys. J. 106 (2014) 2275–2282.
[109] B. Fendler, M. Zhang, L. Satin, R. Bertram, Synchronization of pancreatic islet oscillations by intrapancreatic ganglia: A modeling study, Biophys. J. 97 (2009) 722–729.
[110] A. Loppini, M. Braun, M.G. Pedersen, Mathematical modeling of gap junctional coupling and electrical activity in human β-cells, Phys. Biol. 12 (2015) 066002.